Second Semi-Annual Progress Report:

DESIGN AND APPLICATION OF ELECTROMECHANICAL ACTUATORS FOR DEEP SPACE MISSIONS

Submitted to:

NASA
Marshall Space Flight Center EP64
ATTN: Mr. John R. Cowan

Prepared by:

Dr. Tim A. Haskew
Assistant Professor
Department of Electrical Engineering

Dr. John Wander
Assistant Professor
Department of Mechanical Engineering

College of Engineering
The University of Alabama
Box 870286
Tuscaloosa, AL 35487-0286

Reporting Period:
8/16/93 - 2/15/94

BER Report No. 605-163

Tim A. Haskew
Project Director, Co-Principal Investigator

John Wander
Co-Principal Investigator

TABLE OF CONTENTS

I. EXECUTIVE SUMMARY

This progress report documents research and development efforts performed from August 16, 1993 through February 15, 1994 on NASA Grant NAG8-240, "Design and Application of Electromechanical Actuators for Deep Space Missions." Following this summary, are four report sections: Motor Selection, Test Stand Development, Health Monitoring and Fault Management, and Experiment Planning.

I.1. Research Personnel

Over the entire course of this project, two faculty members, six graduate students, and four undergraduate students have been involved. These individuals are listed below:

1) Tim A. Haskew*, Project Director, Co-Principal Investigator
2) John Wander*, Co-Principal Investigator
3) Kris Cozart*, M.S. Student, Mechanical Engineering
4) Sumit Bhattacharyya, M.S. Student, Electrical Engineering
5) Ramomohan Challa+, M.S. Student, Computer Science
6) Stuart Payne, M.S. Student, Mechanical Engineering
7) Thomas Salem*+, Ph.D. Student, Electrical Engineering
8) Yoon Gyeoung Sung, Ph.D. Student, Mechanical Engineering
9) Stanley McCarter, B.S. Student, Electrical Engineering
10) Sean McGraw, B.S. Student, Electrical Engineering
11) Felix Naylor, B.S. Student, Electrical Engineering
12) Chris Nielsen, B.S. Student, Electrical Engineering

(*) - currently funded on project
(+) - completed a graduate degree on this project

One important point to make is that two students listed above, Challa and Salem, have both completed M.S. degrees through work on this project. Others are nearing degree completion. The entire EMA research group holds weekly meetings in order to coordinate our efforts and provide students with the opportunity to present their work in a formal setting.

I.2. Technology Transfer

As previously mentioned, through efforts on this project, two M.S. theses have been written, accepted, and successfully defended:

> Thomas Eric Salem, *Prime Mover Selection for Electromechanical Actuation in Thrust Vector Control Applications*, Master of Science Thesis, The University of Alabama, 1993.
>
> Ramomohan Challa, *Design of a Computer System to Test Roller Screw Actuators*, Master of Science Thesis, The University of Alabama, 1994.

Additionally, two more theses are presently in the final stages of preparation:

> Sumit K. Bhattacharyya, *Motor and Control Strategy Selection for Electromechanical Thrust Vector Control Applications.*
>
> Kris Cozart, *Design and Control of a Roller Screw Test Stand.*

While theses and dissertations constitute a vital component of technology transfer, the most extensive means are through publication in technical journals. Presently, three manuscripts are in progress. The titles and journals for submission are provided:

> "Motor Selection for Electromechanical Thrust Vector Control Actuation," *IEEE Transactions on Aerospace and Electronic Systems.*
>
> "An Adaptive Kalman Filter Approach to Fault Detection in DC Motors," *IEEE Transactions on Energy Conversion.*
>
> "Numerical Modeling of Disk Springs," *ASME Journal of Dynamic Systems, Measurement, and Control.*

As our work progresses, particularly with experimental results available from the test stand, we expect many more conference and journal submission.

I.3. Schedule of Upcoming Accomplishments

For informational purposes, a tentative schedule of expected near-term accomplishments has been compiled:

- First experiments beginning on test stand - May 2, 1994
- Laboratory validation of fault detection and quantification for an armature short-circuit - May 16, 1994
- Test of prototype fault detection hardware breadboarded from commercially available components - August 1, 1994

II. MOTOR SELECTION

Three specific motor types have been considered as prime movers for TVC EMA applications: the brushless dc motor, the permanent magnet synchronous motor, and the induction motor. All three have been confined to three-phase configurations. Previously, we have reported the criteria that impact motor selection. The fundamental finding was that, in general, the primary performance issues were energy efficiency and thermal dissipation (rotor heating). In terms of all other issues, the three motor types were found to compare quite equally. In light of these findings, we instituted a detailed simulation study to provide basepoint comparisons, primarily on energy efficiency. Additional, though not highly detailed, thermal analysis was performed.

II.1. Initial Studies Without Controller Effects

To provide an initial estimation of machine efficiencies in TVC applications, rough equivalents of the General Dynamics and MSFC actuator motors were compared. The simplified nozzle/actuator system arrangement considered is presented in Figure II.1. The acceleration and weight vectors are separated by 30 degrees. Using a 10:1 gear reduction and 6 mm screw lead yielded a load torque of 55 N-m. The effective inertia of the system was dependent on motor, screw, and transmission inertias as well as gear reduction, screw lead, and load mass. Typical values available in the literature were used. It was readily apparent that the system inertia was dominated by the load mass (4,400 kg) term. Thus, the effective inertia employed for simulation was 0.0016 kg-m^2.

A sinusoidal input command for linear displacement of the actuator was employed, as seen in (II.1).

$$x = X_{max} \sin(\omega t) \tag{II.1}$$

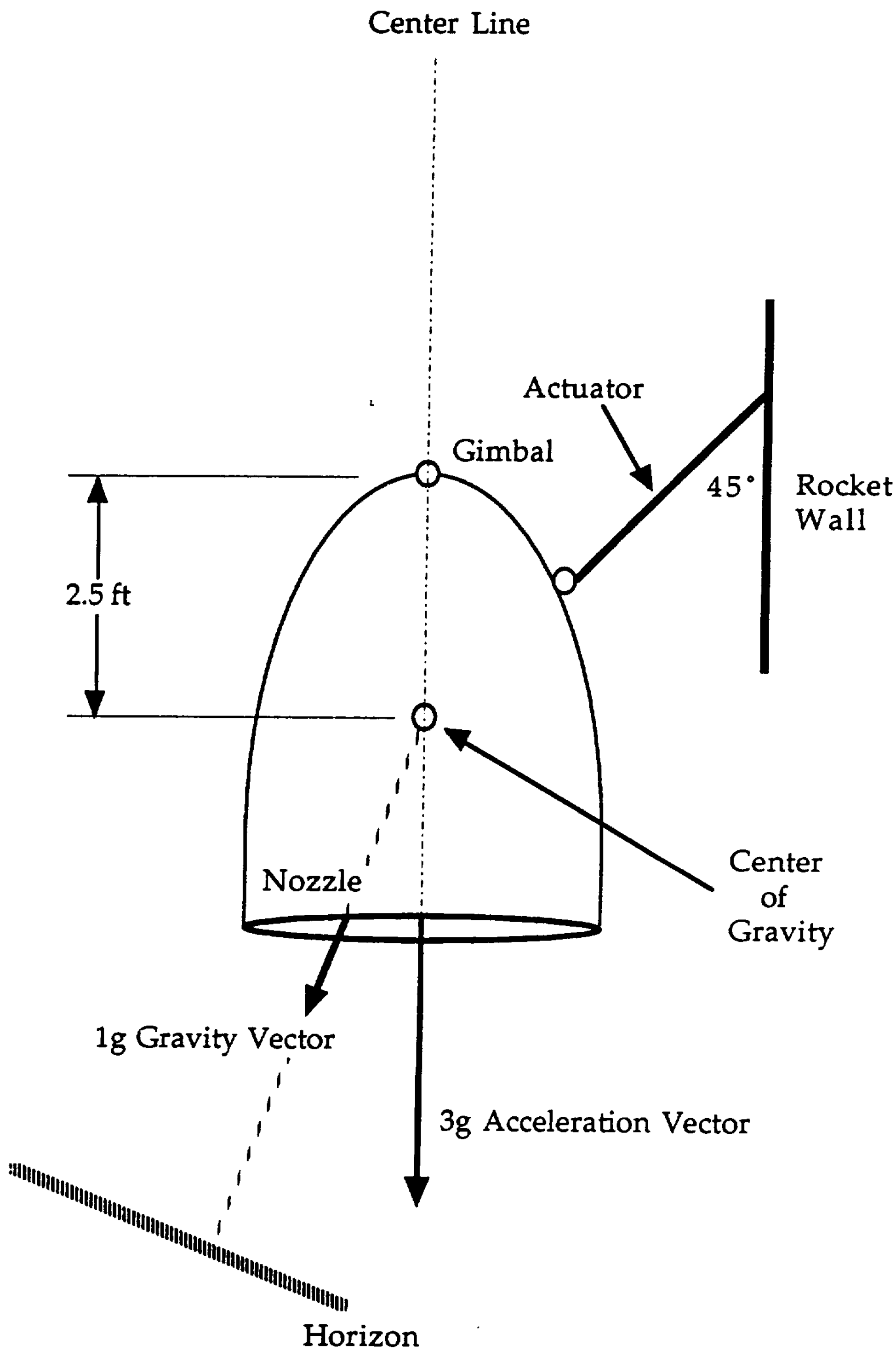

Figure II.1. Nozzle/Actuator Arrangement.

This form of input motion trajectory provides a reasonable test and forms a basis for use of Fourier series expansions of more complicated trajectories. From (II.1), the machine rotor angle (θ), velocity (ω), and acceleration (α) can be easily calculated. Rotational torque losses were neglected, thus the developed torque for either motor can be found as shown in (II.2).

$$T_{dev} = T_{load} + J_{eff}\alpha \tag{II.2}$$

The developed torque allows adequate input to a numerical simulation of motor performance. The induction machine data was taken from information supplied by General Dynamics. The armature resistance was 0.0298 Ω/phase, the rotor resistance was 0.0267 Ω/phase, and the core resistance was 31.65 Ω/phase. Since the core resistance was so large, it was neglected. The self-inductances of the stator and rotor were 28.8 and 24.3 μH/phase, respectively. The magnetizing inductance was 395 μH/phase. The brushless dc motor data was extracted from information provided by MSFC. The stator resistance was 0.04 Ω/phase, and the stator inductance was 270 μH/phase. The motor constant was 0.244 N/A or Vs/rad.

Torque control of the dc motor was accomplished with ideal armature current control. The induction motor was controlled at a constant slip with variable input voltage and frequency. Note that this is not field-oriented control, as General Dynamics has proposed. An additional note is that steady-state circuit analysis techniques were employed. However, this approximation is reasonably accurate due to the fact that the period of the sinusoidal linear displacement is extremely large compared to the electrical and mechanical time constants of the system.

Figure II.2 shows the instantaneous efficiencies of both machines with a sinusoidal input sequence of 1.5 inches in magnitude at a frequency of 0.1 Hz. Obviously, the BDCM is more efficient. The simulations were executed over a wide range of input trajectory magnitudes and frequencies; the results were similar in all cases. However,

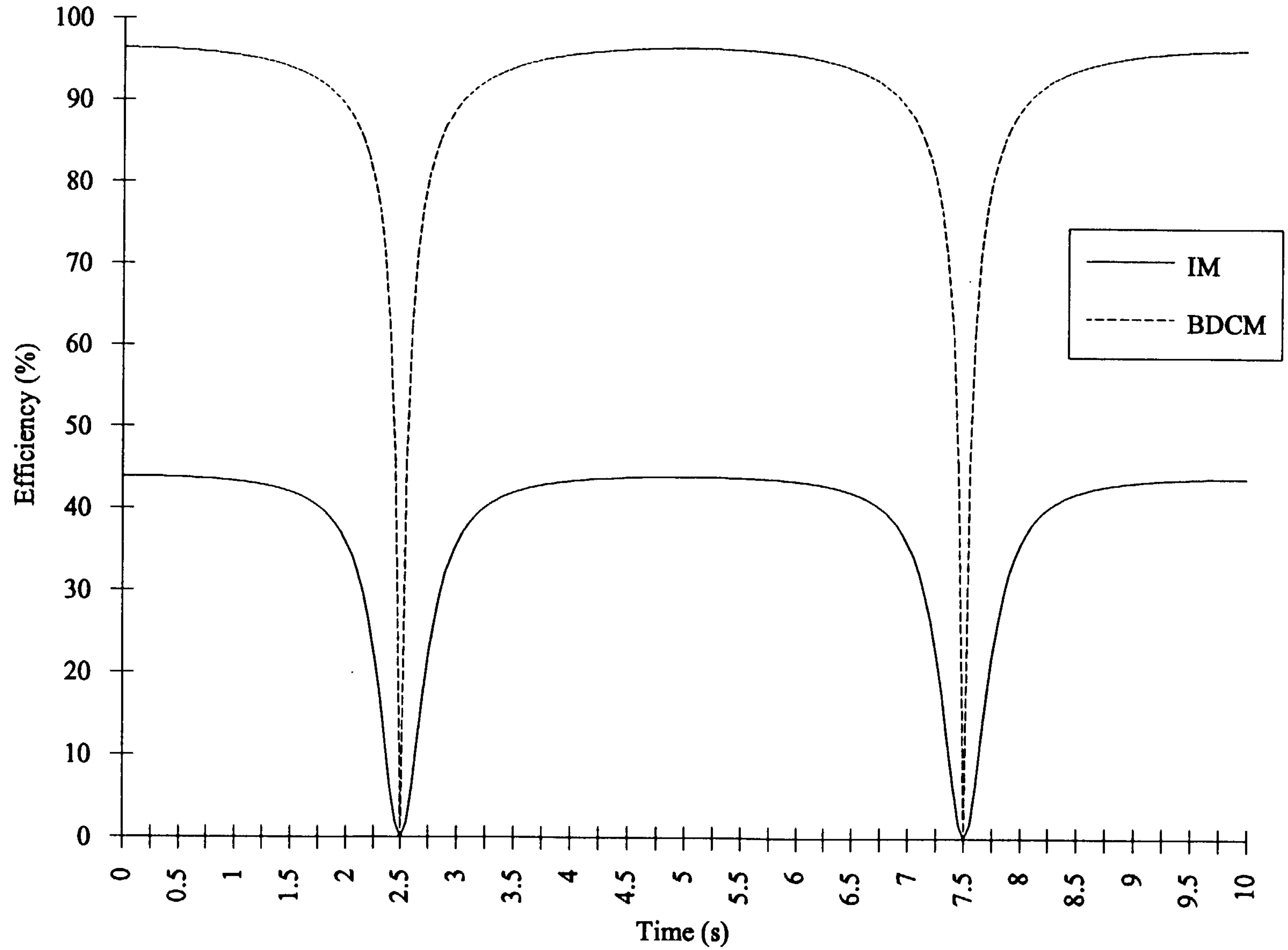

Figure II.2. IM and BDCM Efficiency Comparison.

with the implementation of field oriented control, the IM efficiency can be driven much higher. Thus, investigation into the performance with realistic control action was considered.

II.2. Dynamic Motor/Controller Simulation and Studies

To address the effects of control strategy, full dynamic motor/controller simulations were written. All three motor types were simulated. Pulse-width-modulation (PWM) and hysteresis control strategies were employed with each motor type. Thus, six base case simulations were implemented.

In all simulations, the power semiconductor switches were modeled as ideal. Thus, no losses were associated with the drives. This was intentional so that switching device efficiencies were not a factor in our motor/control strategy evaluations. The same input position trajectory previously presented was used in these simulations as well. However, in these more advanced simulations, this constituted a reference signal input to the controller rather than an actual output signal. Again, the input was varied over a wide range of input magnitudes and frequencies.

Simulations were performed on similarly rated machines of each of the three types for which manufacturer's and experimental data has been published. All machines were rated at approximately 1 Hp. In general, the PWM drives proved to be the most efficient for all three machines. In light of this, investigation into hysteresis current control was discontinued. Thus, we were concerned with the brushless dc machine and permanent magnet synchronous machine operating under PWM current control and the induction machine operating under PWM field-oriented control.

Figures II.3, II.4, and II.5 show the efficiencies of the three machines versus both angular displacement amplitude and frequency of the sinusoidal input. The "jitter" on the plots is resultant from torque pulsations that occur in the absence of current limiting.

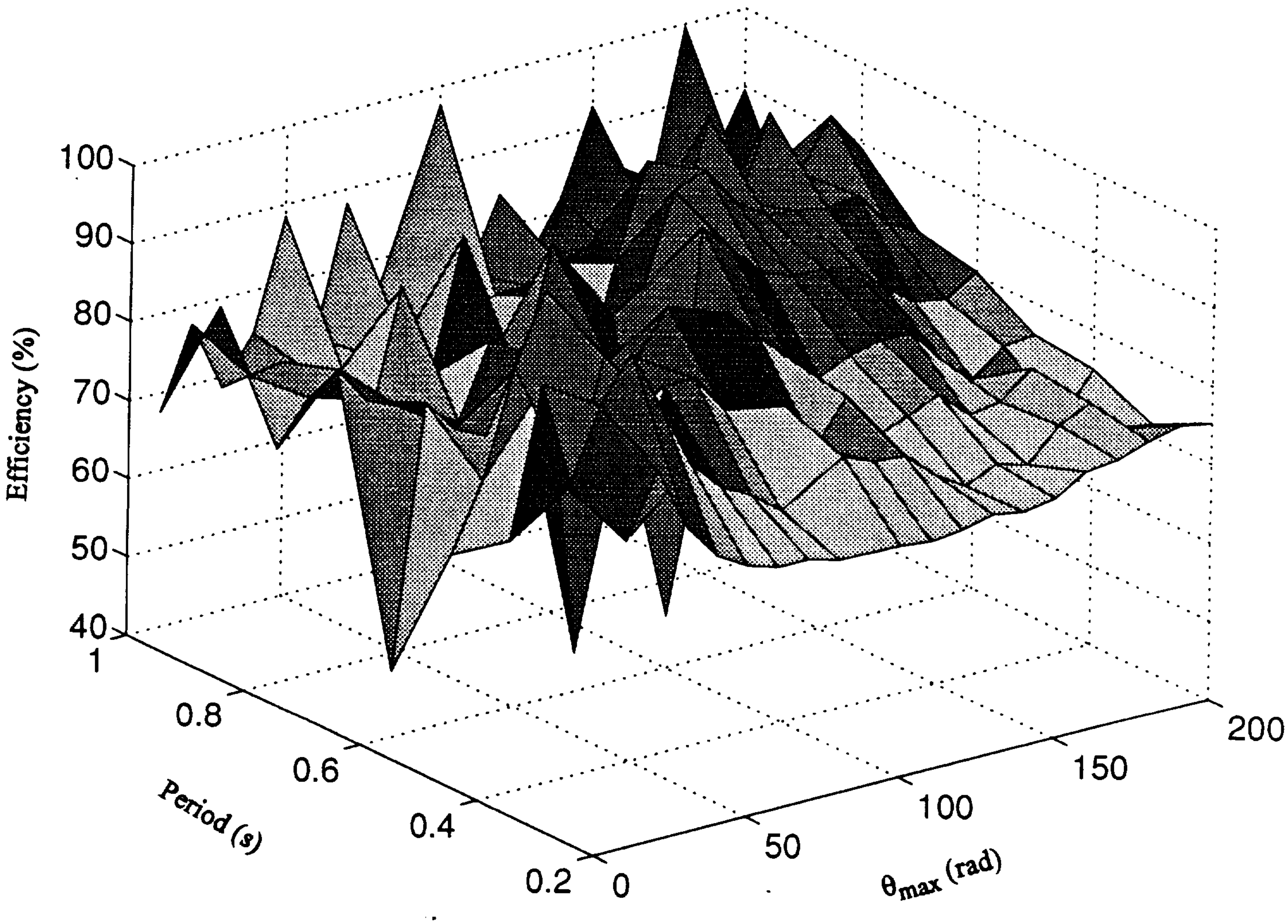

Figure II.3. BDCM Efficiency.

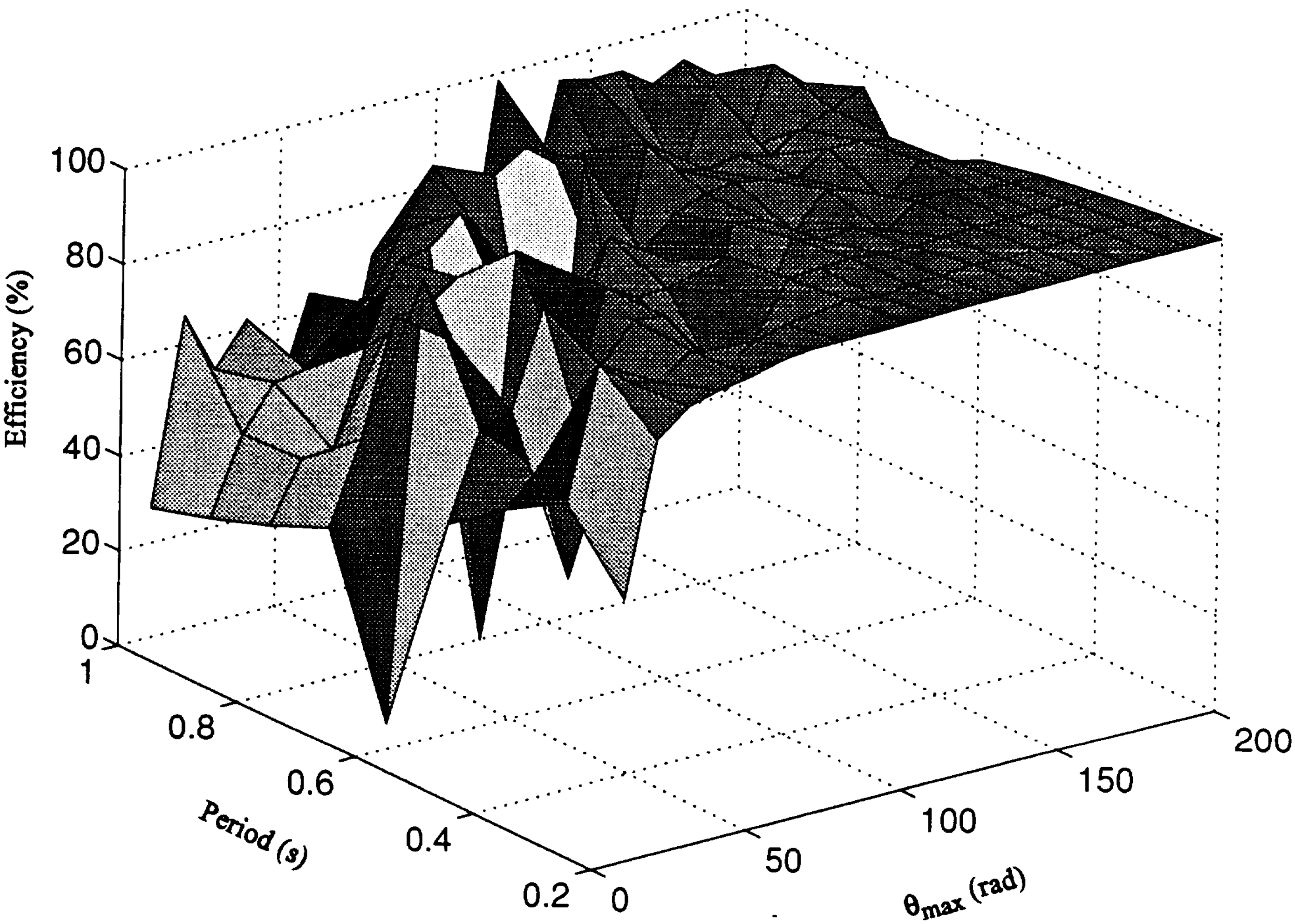

Figure II.4. PMSM Efficiency.

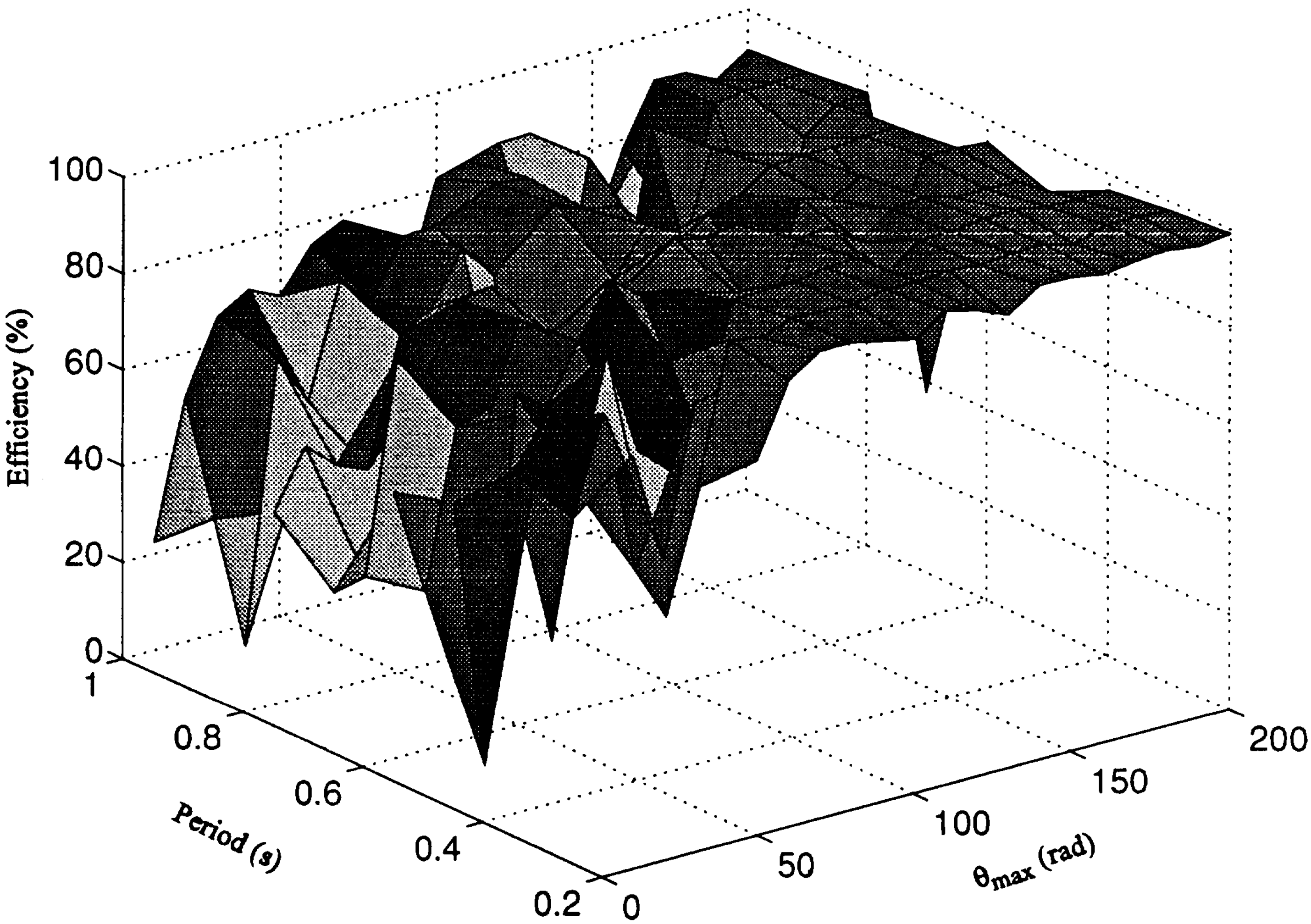

Figure II.5. IM Efficiency.

However, the general trend shows that the brushless dc motor is generally more efficient in the region that is typical of thrust vector control applications.

II.3. Recommendations

From the foregoing brief presentations of our studies, we recommend use of the brushless dc motor or permanent magnet synchronous motor for electromechanically actuated thrust vector control where rotor temperatures will be sufficiently low to prevent demagnetization. Not only do these machines offer higher efficiency, but they also provide higher torque to volume and torque to mass ratios than induction machines. It is intended that a technical article will be submitted for publication in a technical journal on this topic in the near future. Additionally, we are currently extending our efforts to include efficiencies of the various components within the motor drives.

II.4. Hybrid Actuator Development

Previous efforts of research in the area of motor selection have resulted in the recommendation for using the brushless permanent magnet direct current machine as the prime mover in the thrust vector control application. This recommendation resulted from the consideration of various machine technologies for this specific application. During this review process, it was recognized that different applications could warrant a different choice in the prime mover; for example, a stepper motor would probably be a better choice for an application that required a high degree of accuracy in placement position.

Consideration was also given to the improvement and development of the overall concept and design of electromechanical actuators. Some of the critical factors in the design of these systems include the system reliability, efficiency, total mass and inertia.

From the information gained in the study of the prime mover candidates and the concepts related to system improvements, a new hybrid actuator system has been conceptualized.

The proposed hybrid actuator system consists of an induction machine with the traditional rotor replaced by the nut of a roller screw which has been converted to function as a rotor. This design allows the prime mover to directly drive the roller screw and has several advantages over the current electromechanical actuation systems. The stator may also be equipped with a second winding to produce a linear force component in addition to the rotational force. This developed dual force of the machine presents intriguing possibilities for utilization in the actuator design.

II.4.1. Hybrid Actuator Description

The basis for the hybrid actuator design stems from the initial investigation into why rotational machines were being utilized for producing linear motion when in fact there already exists machine technology capable of directly producing linear motion. Linear machines come in a variety of configurations utilizing induction as well as direct current technology. One of the most interesting candidates was the tubular linear induction machine, which contains a shaft wrapped with a conducting surface inside a cylindrical stator capable of producing linear motion. However, there are features intrinsic to this design, primarily its force production capability, which prohibit its utilization in the thrust vector control application.

Another intriguing candidate, which is similar in nature to the tubular linear induction machine, is the rotary linear induction machine. This recently developed machine contains dual stator windings that produce rotational and linear forces on the rotor, which is again a shaft wrapped with a conducting surface. Since the stator coils are separately driven, the machine is capable of purely rotational motion, purely linear motion or a combination of both rotational and linear (helical) motion. It is interesting to note that the rotor shaft does not need to be solid, in fact a hollow steel shaft wrapped in a conducting thin sheet of copper has been demonstrated in the literature.

The conceptual design of the hybrid actuator system consists of combining the rotary linear induction machine technology with roller screw mechanics to produce an improved actuator system. The shaft of the machine would functionally be the nut of the roller screw as well as the rotor. This would also probably entail utilizing a solid nut versus a split nut on the screw, enhancing the load capability and reliability while maintaining the features of the pre-load on the split nut by proper control action of the linear force component on the solid nut. The design would allow for the required torque development to be realized with the rotational force component, which would be directly translated into linear motion by the rotor, thus creating a directly driven system.

The technology of the induction machine is viewed as a necessary first step, primarily due to cost effectiveness, in demonstrating the feasibility of this design approach. However, once demonstrated, this technology could incorporate the brushless permanent magnet direct current technology to produce an even better actuator system.

II.4.2. System Advantages

Perhaps the most significant advantage to this hybrid design is the reduction in total system mass. By combining the rotor of the machine with the nut of the actuator, the mass of the rotor is eliminated from the system. Utilizing the machine to directly drive the actuator eliminates the requirement for a linking gear train system thus removing the mass associated with the gear train. Furthermore, since the gear train would be eliminated there would most likely be a reduction in mass associated with a reduced housing frame structure of the actuator system.

There are several opportunities for overall system efficiency to be enhanced with the hybrid design. First of all, since the hybrid system has a lower mass, the amount of energy required to carry the actuator as payload would be reduced. This may be a significant enhancement depending on the application requirements for carrying the actuator system; for example, in the thrust vector control application, this reduction in mass is significant and correlates to energy savings and increased Shuttle payload capacity. Secondly, the efficiency of the actuator itself would be enhanced by the reduction of mass associated with rotational inertial (i.e. the elimination of the rotor and gear train mechanism). This reduction would allow for more of the machine energy to be exhausted on moving the roller screw assembly itself rather than on rotating extraneous mass. Finally, the issue of efficiency needs to be evaluated in light of application specific duty cycle requirements. Although the induction machine technology has a lower efficiency rating with regard to energy conversion than that of the brushless permanent magnet direct current machine technology, this would not be a critical factor for applications with light duty cycle requirements.

Overall actuator system reliability would be enhanced by the hybrid design. By eliminating several components in the design, reliability would be improved. Elimination of the linking gear train enhances reliability not only by removing the failure potential of the gear mechanism itself, but also eliminates the failure potential of the lubrication required for the operation of the gear train. By using a solid nut on the roller screw and as the rotor, the design would have an enhanced reliability compared to actuators using a split nut. The reliability would also be enhanced by the use of the conducting thin sheet on the nut as opposed to the traditional rotor bars or rotor windings, which are susceptible to stress failures. The induction machine technology is also known for having a greater reliability in high temperature applications in comparison to the brushless permanent magnet direct current technology.

As previously stated, this conceptual design utilizing the induction machine technology would be a necessary first step towards development of this design with the permanent magnet technology. If the permanent magnet design were developed, a tremendous advantage could be realized by the potential for eliminating the Hall effect sensor, traditionally used for triggering the electronic drive system of the machine. This sensor, which is currently one of the drawbacks in the brushless design, would not be required since there is a direct coupling of linear to rotational motion, and the linear position sensor could provide the necessary rotational position information to the motor drive.

II.4.3. Recommendations

Further study and investigation of this conceptual design is recommended. A systematic approach to the development and demonstration of the principles of this design is warranted. The principles of induction machine technology should be utilized in the initial development stage as a cost effective means to demonstrate this design, while reserving the future potential of incorporating the permanent magnet technology into the design.

III. CONSTRUCTION OF THE EMA TEST STAND

Since the first annual report on this work in August 1993, the conceptual design of the test frame has become a detailed mechanical design. The final design is very similar to the conceptual design except for a few improvements. All parts of the test frame itself are either completed or currently being machined. Work is currently being done on the design of the nut carrier assembly and the related hardware and instrumentation.

III.1. Site Preparation

A site for the test stand has been chosen in the Electric Machines Lab at the University of Alabama. The controlled climate room is provided with cement mounting blocks for heavy equipment. These blocks support steel frames that will be used to hold the bottom of the test stand frame at a height of three feet above the floor. The test stand will be mounted on two supports, one at either end, with the under-slung nut carrier riding between the supports. Arranged in this way, there will be easy access to the test area and additional support for end-mounted motors or hydraulics. The facility is well equipped to support this experimentation with a variety of electrical power options and a two-ton overhead crane available.

III.2. New Developments

Among the design changes made to the test stand since our last progress report is the addition of more mounting holes in the side beams. These additional holes allow the movable end beam to be attached in a greater number of positions than previously. With this change the movable end beam can move from full forward to full back in three inch increments. To help make use of these additional positioning possibilities a keyway was added down the center line of the side beams and the end plates to keep the bearing box axes in line. This will also aid in the initial setup of the test stand. The final test frame drawings appear in the Appendix A.

During the project meeting in November at NASA Marshall Space Flight Center, several improvements in test stand design were suggested. In particular, bearing box alignment aids were added in the form of tooling pins located in the end beams. In addition, it was decided that NASA would provide the EMA team with a set of bearings identical to those being used in the NASA TVC actuator. Using these bearings to support the screw will allow the test stand to use a modified NASA bearing housing design and end-of-screw design. This modification saves design time and will allow testing the same screw bearing combination as used in the EMA. This modification does more than save time and effort. By copying the NASA screw-end machining, the possibility of driving the screw with the main drive gear as in the actuator design is left open. In the future we may more accurately simulate the dynamics of the EMA by adding the main drive gear and the parallel electric motors to simulate redundant actuation. The initial experiments, on the other hand, will utilize an electric motor coupled to the end of the screw and a spacer in place of the sun gear (see Figure III.1).

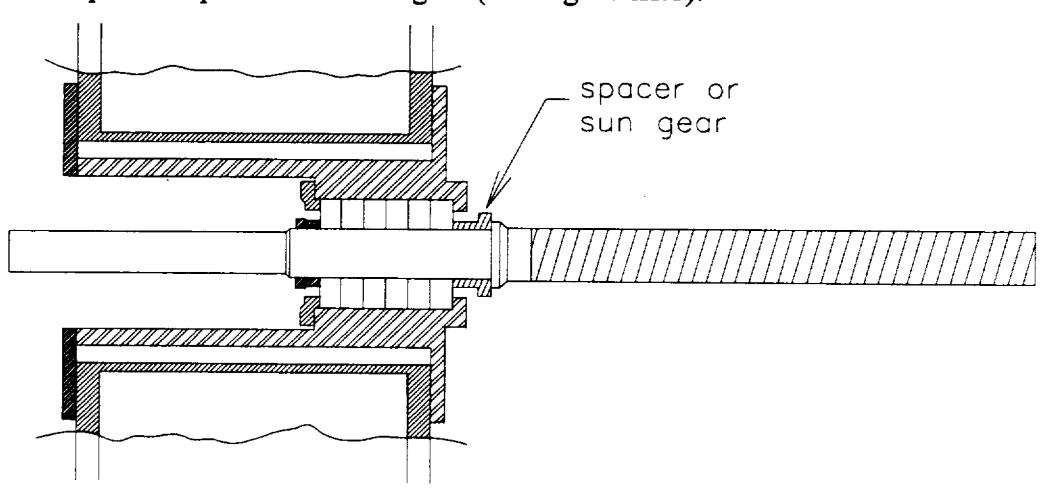

Figure III.1. Bearing Box and Roller Screw.

A linear bearing system and carrier were designed to support the roller screw nut and prevent rotation while allowing it to travel in the axial direction. The original design called for a one inch double shaft fully supported assembly. A single two inch shaft system will be used instead, primarily because of the cost reduction in both the machining and the hardware itself. The larger diameter shaft will allow a small portion to be unsupported and moved over the end plate to be closer to the end beam holding the roller screw. The overhang allows the center of the bearing rod to be more aligned with the center of the threaded section of the roller screw and allows full travel of the nut as shown in Figure III.2. This configuration requires fewer mounting holes in the side beams thus reducing machining cost. Note that two pillow blocks are needed per side, because of the self-aligning nature of the linear bearings, to support both the static gravity moment generated by the thrust load cell, pipe, and axial coupling and to support the inertial moment generated by the accelerating mass of the carrier.

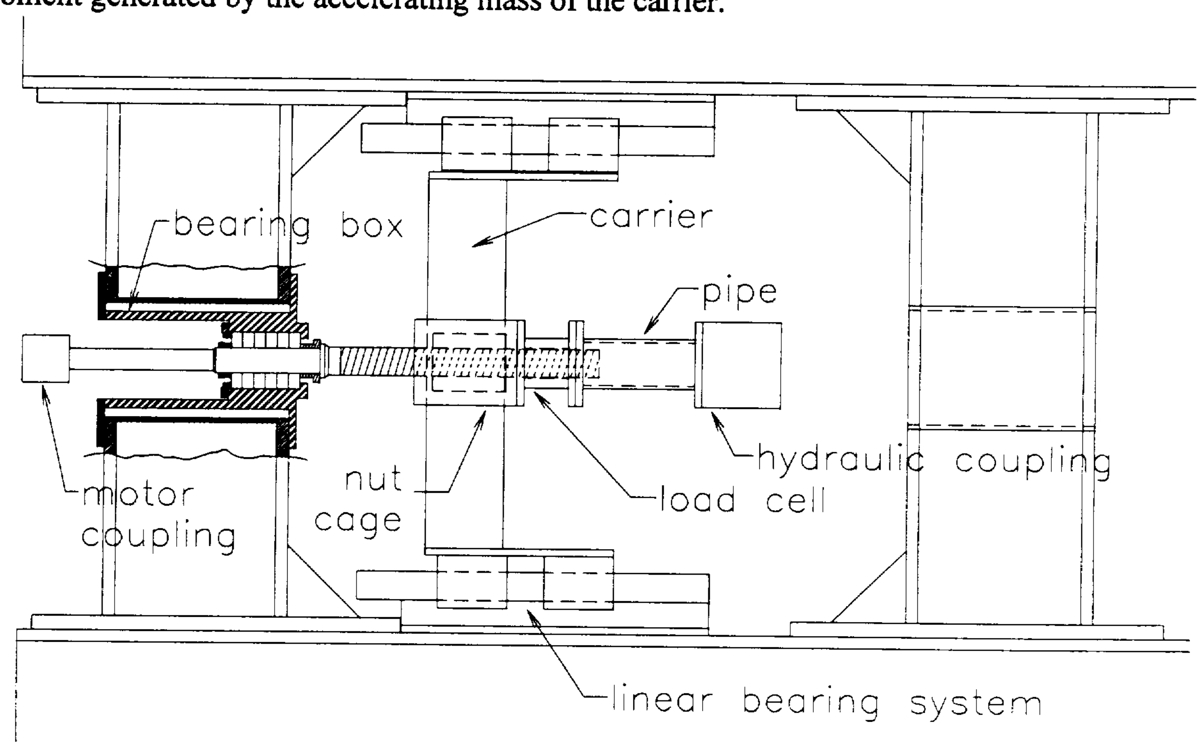

Figure III.2. Scale Drawing of Roller Screw Test Stand.

The carrier has also been redesigned. In the past the carrier was designed to be reconfigured for different experiments. The design now in progress utilizes a W8x21 I-beam, mounted between the linear bearings, as a permanent base for measurements and transmitted loads. In the axial loading experiment the nut cage is bolted to the carrier by way of load cells to measure reaction torque. In any experiment with a transverse load applied, the load must be born by the screw and not the carrier. So for these experiments the nut cage will be attached to a linear slide, again by way of the load cells, which allows the screw to move in the transverse direction while bearing any generated reaction torques. See Figure III.3.

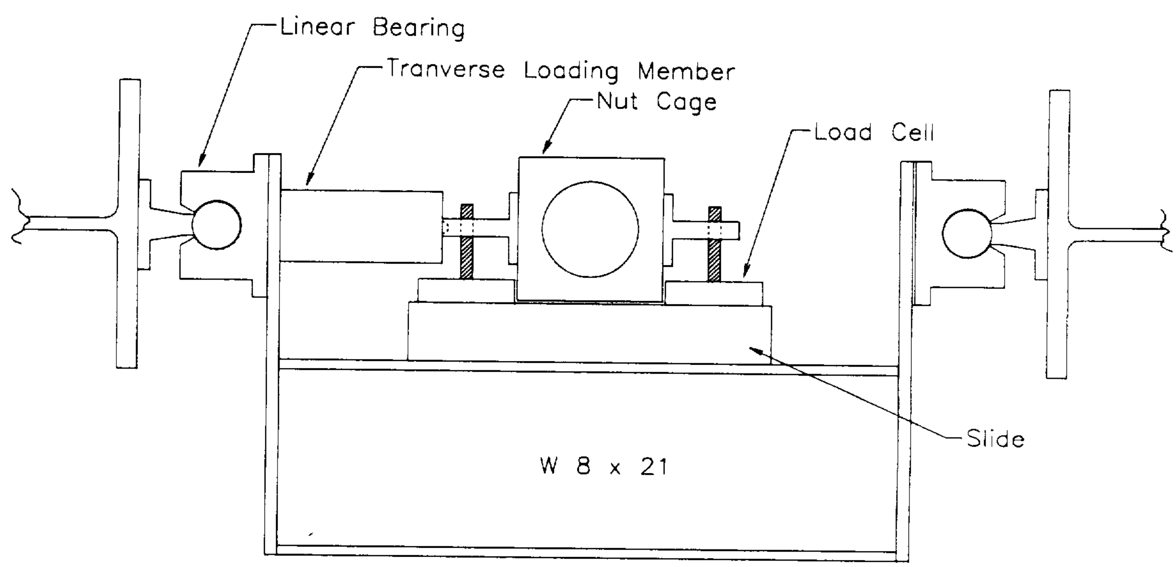

Figure III.3. Scale Drawing of Carrier Assembly.

Figure III.3. shows additional developments since our last report. The load cells mounted beside the nut cage have been respecified and detailed designs for the slide assembly have been completed. The load cells prevent the nut cage from rotating and can be used to measure reaction torques generated with the tension and compression forces. Note that the transverse loading member (TLM) will not hinder torque measurement since part of the design requirements of the TLM is to allow small vertical deflection at the torque arm. The rounded right end will allow the resulting angular change between the TLM and the nut cage. Also note that the specified reaction torque load cells are designed to remain accurate under application of significant side and eccentric loads. This ability to bear high side loads is necessary in order to accelerate the carrier assembly.

Several of the subassemblies recently completed and going into construction are being produced in association with a manufacturing processes course recently added to the engineering curriculum at The University of Alabama in cooperation with Shelton State Community College. The detailed design of the transverse loading member, the transverse slide and the axial loading coupling that allows for small misalignments between the hydraulic loading cylinder and the roller screw have been completed by students under the supervision of project personnel. These designs are currently in review. These parts will also be fabricated at Shelton State in association with this course resulting in a savings to the project and the broader impact of this project on higher education in Alabama. The initial student drawings are reproduced in Appendix B.

The test stand will be operated through an IBM compatible PC with analog and TTL level digital inputs and outputs. The basic system has been specified based on a careful review of available hardware and software and the test requirements. This review has been documented in a Masters thesis completed early in 1994 [III.1]. A PC has been selected and the system indicated in the proposal to build the test stand is being purchased. The items being purchased and the purchase prices are listed in Table III.1.

Table III.1. Computer Hardware in Acquisition

Description	Cost
Computer	
4DX-33 Intel 486 PC 4 MB RAM, 212 MB 13 mx IDE Hard Drive, 3.5" floppy,14" color CrystalScan 1024 NI, 5 16-Bit ISA Slots, keyboard, etc.	$1,495.00
	$1,495.00
Data Acquisition and Control Peripherals	
CIO-DAS 16/330i, 16 channel A/D board*	$719.10
CIO-DDA 06, 6 channel analog output board*	$314.10
CIO-SSH-16, 4 channel simultaneous sample and hold*	$351.10
C37FF-2, 37 connector ribbon cable*	$22.50
C37FFS-5*	$27.00
CIO-MINI37*	$44.10
ENC 19 by 7 by 3	$59.00
	$1,536.90
	$3,031.90

* - The prices of these items reflect 10% university discount.

The conceptual design called for two load cells to be mounted beside the roller screw to measure the main thrust applied to the nut. Upon inquiry with load cell vendors it was found that a single load cell with a bore sufficient to allow the screw to pass down the middle of the load cell could readily be provided. The bolt hole patterns required of the load cell to mount between the loading pipe and the nut cage have been provided to Sensotec along with other specifications and the load cell is in development. This redesign will result in a savings to the project and a better instrument for measurement of axial load. In addition, it was discovered that the load cells originally specified for the measurement of reaction torque would measure compression only. Though these could be used they would require a transverse load be applied in proportion to the torque on the nut. Coupling these variables is unacceptable given the experimental goals. Load cells that can measure both tension and compression have been respecified at some increase in cost. Finally, the transverse load cell has been specified. The final decision about signal amplification will be postponed until all the instrumentation has been reviewed and output levels are compared.

III.3. Task Schedule

Progress toward completion of the test stand has been steady. Table III.2 gives a listing of the current and completed tasks along with an estimate of future completion dates. Items to be purchased should arrive by the completion dates indicated.

Table III.2. Test Stand Development Status

Task/Item	Status	Expected Completion Date
frame: end beams	completed in-house	complete
frame: side beams	quoted, delivered being machined	2/21/94
main frame assembly and mounting at test site	awaiting side beams	2/28/94
end-of-screw machining	complete except thread and keyways	2/28/94
main gear spacer	complete	complete
bearing nut and backing plate	NASA designs to be adapted, waiting on thread decision	2/28/94
flanged axial loading pipe	design complete, to be fabricated in-house	3/4/94
main bearing housing	drawing nearly complete, to be machined in-house	3/18/94
nut cage	detailed design in progress, to be machined in-house	3/18/94
nut carrier riding on linear bearings	detailed design in progress, to be fabricated in-house	3/18/94

Table III.2. Test Stand Development Status (continued)

Task/Item	Status	Expected Completion Date
hydraulic and electric actuation system mounting machining	awaiting specification of actuation hardware	3/25/94
linear bearing system, rods, supports and roller bearings	respecified, to be purchased	3/25/94
transverse loading load cell	respecified, to be purchased	3/25/94
torque are load cells	respecified, to be purchasing	4/1/94
torque arm assemblies	detailed design in progress, to be machined in-house	4/8/94
transverse loading systems (2)	design complete, to be fabricated at Shelton State in **ME 383**	4/20/94
transverse slide	design complete, to be fabricated at Shelton State in **ME 383**	4/20/94
axial load coupling to allow misalignments of screw and hydraulic cylinders	design complete, to be fabricated at Shelton State in **ME 383**	4/20/94
hydraulic loading system	in review for purchase	4/20/94
main electric drive motor	in review for purchase	4/20/94
main axial thrust load cell	quoted, special design in progress at Sensotec	4/29/94
computer control and data acquisition system with basic driving software	design complete, in acquisition, basic drivers for instruments in development	4/29/94

The development of the test stand is progressing well. The computer system will arrive soon so that the instrument drivers can be developed and debugged before the stand is complete. The first experiments to be conducted (transverse loading experiments) should begin some time in May.

III.4. References

[III.1] Challa, R., Design of a Computer System to Test Roller Screw Actuators, Masters Thesis, The University of Alabama, January, 1994.

IV. HEALTH MONITORING AND FAULT MANAGEMENT

Specific mathematical details on the approach we have employed for health monitoring and fault management (HMFM) have been reported previously. This approach is based on an adaptive Kalman filter strategy. In general, a bank of filters can be implemented for each primary fault type. Presently under consideration for the brushless dc machine are the following faults:

- Armature Winding Open-Circuits
- Armature Winding Short-Circuits
  (Phase-to-Phase and Phase-to-Ground)
- Bearing Degradation
- Rotor Flux Weakening

At this point, rotor flux weakening and armature short-circuits have received the most attention.

The long-term goal of these efforts will be a hardware prototype of a health monitoring and fault management system that will be capable of detecting impending failures of any one of the above listed types. Additionally, a hardware interface is intended that will allow suitable feedback into power scheduling algorithms within the controller of the redundant motors. This is hoped to mitigate total motor failures or at least minimize failure related effects, such as additional loading placed on operational motors in the presence of a short-circuited brushless dc motor.

As the brushless dc machine exhibits operational characteristics virtually identical to that of classical dc machines operating in the separately excited mode, we have been performing simulation and experimentation on classical dc machines. This approach has been utilized for two specific reasons: the induction of a planned fault is simplified, and the availability of classical machines for modification is great.

IV.1. Simulation Efforts

A detailed presentation of the simulation procedure that has been employed for testing and verification of the HMFM algorithm can be found in our first year annual report. However, a simple illustration is included here. Substantial data was available for a 250 V, 200 Hp dc motor. This data is presented in Table IV.1.

Table IV.1. DC Motor Test Data.

Quantity	Value
Armature Resistance	0.012 Ω
Field Resistance	12 Ω
Armature Self-Inductance	0.35 mH
Field Self-Inductance	9 H
Armature-Field Mutual Inductance	0.18 H
Moment of Inertia	30 kg-m^2

For algorithm evaluation, a state model for the machine was simulated under steady-state running conditions with a load torque of 2375 N-m. At 0.25 s of simulation time, the field flux was reduced by 30%. The simulation outputs were noiseless system measurements of armature current and rotor velocity. Terminal voltage and load torque were treated as pseudo-measurements. Onto the measurements, zero mean white noise was injected. The noise standard deviations were 75 A and 5 rad/s for the armature current and rotor velocity, respectively.

These noisy measurements and the system data were supplied to a software version of the adaptive Kalman filter. Figure IV.1 shows the filter's quantitative classification of the faulted motor constant. Note that when the output of the adaptive Kalman filter is low-pass filtered, a reasonably accurate estimate of the motor constant is available. Additionally, output includes measured quantities with reduced noise components. Thus, the system can be used for more accurate feedback in high accuracy actuation applications as well as for fault diagnosis and classification in a fault management system.

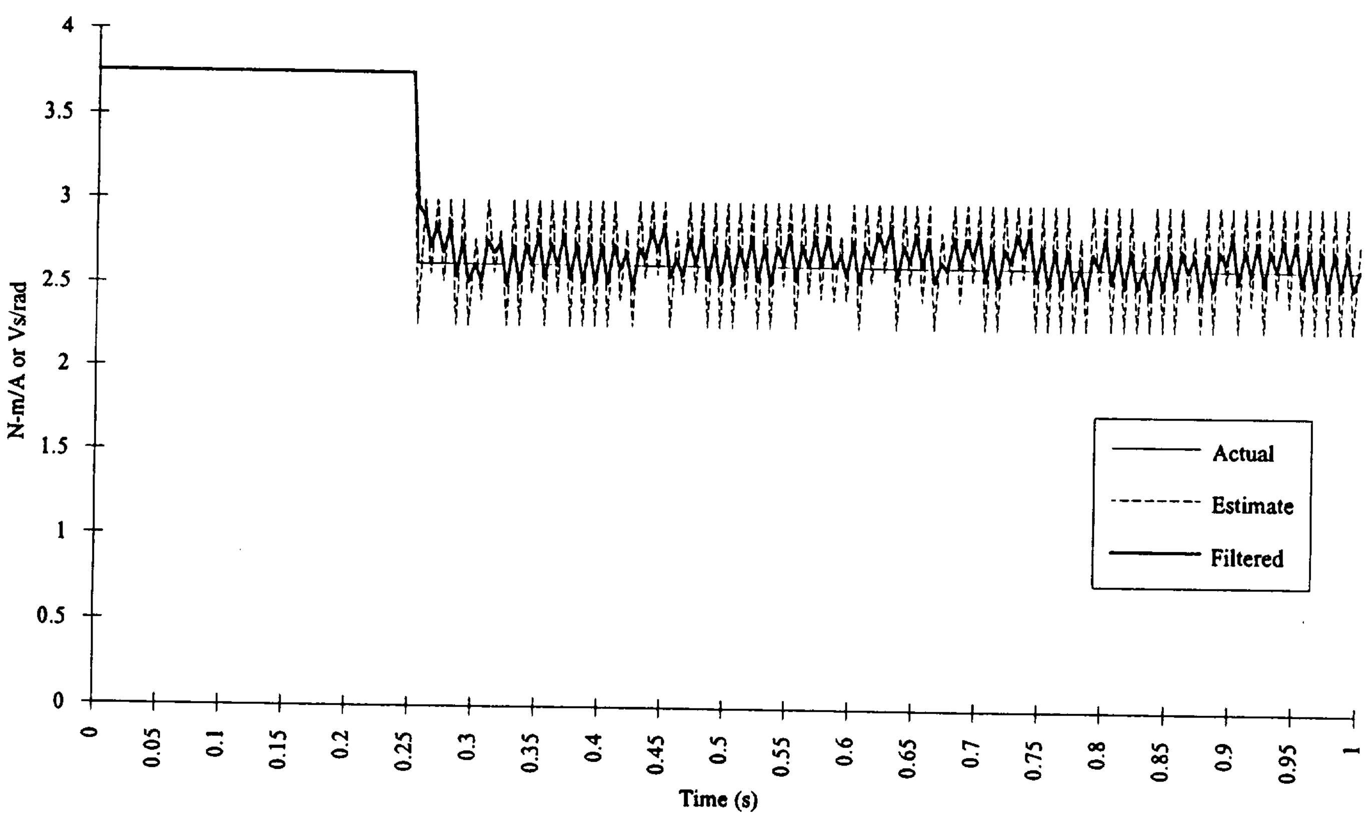

Figure IV.1. Motor Constant Estimation.

IV.2. Laboratory Validation

In our last report, explicit detail on the simulation efforts was provided. Such was briefly documented above. However, at this time, we have laboratory validation of the HMFM algorithm. We have approximately six fractional horsepower dc machines of identical models appropriate for in-house experimentation of this nature. The laboratory configuration used is presented in Figure IV.2.

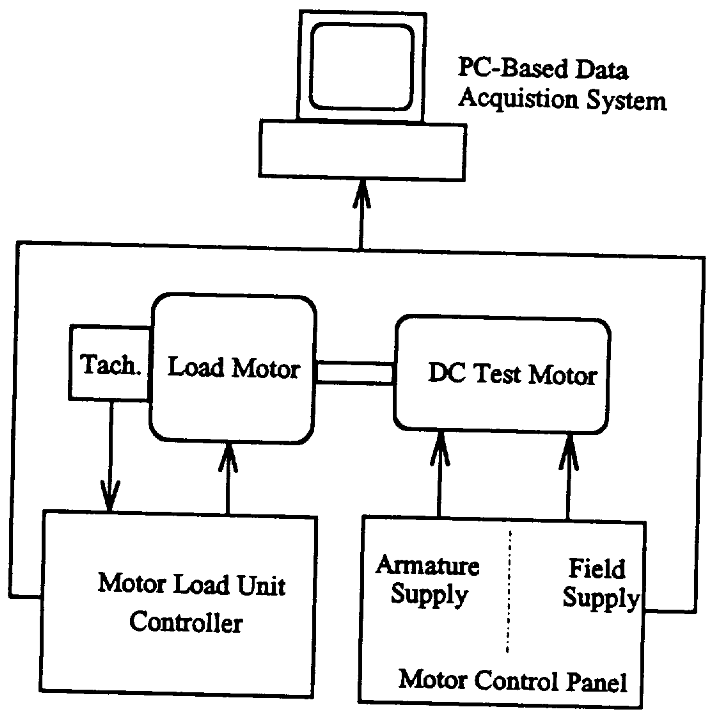

Figure IV.2. Experimental Configuration.

For laboratory validation of the HMFM algorithm, laboratory testing was performed to gather the required motor data which was not included on the nameplate. This data was then used to construct the adaptive Kalman filter for identification of field flux weakening.

A single motor was connected in a separately excited configuration and run under steady-state. 0.27 seconds after data acquisition was initiated, the field current was reduced to 89% of the prefault value to simulate a field flux reduction such as may be introduced by overheating in a BDCM. Figure IV.3. shows the filter output and measured values of the armature current, and Figure IV.4 shows the actual and estimated motor constant.

It is important to note that the induced flux change was extremely rapid, which is unrealistic in a worst case sense. Thus, the low-pass filter on the output of the Kalman filter can be adjusted to reduce the jitter even further. This will remove the fast transient in the current estimate, but will provide a much more accurate steady-state estimate. This should not be problematic however, as actual rotor flux reduction will be a slow process.

IV.3. Continuing Efforts

The laboratory validation for flux weakening disturbances was performed off-line with previously gathered data. However, we are presently designing prototypical hardware for real-time processing. Additionally, we are in the process of performing laboratory validation of the algorithm for detecting and quantifying armature short-circuits. The algorithm has already been validated through simulation, and modifications have already been made on a motor such that we will be able to introduce controlled short-circuits within the armature windings. The prototype will be easily reprogrammed for all fault types.

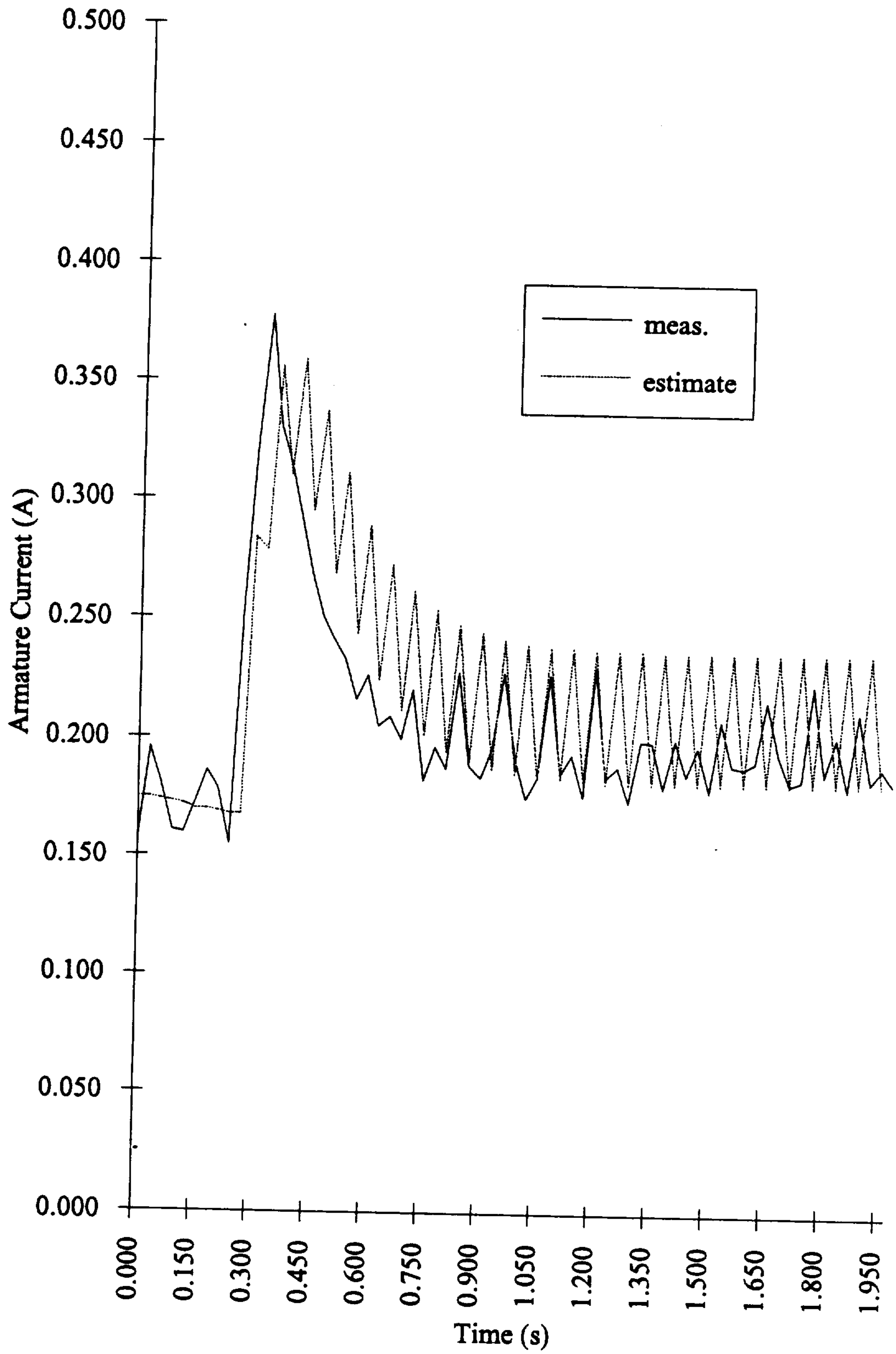

Figure IV.3. Measured and Estimated Armature Current.

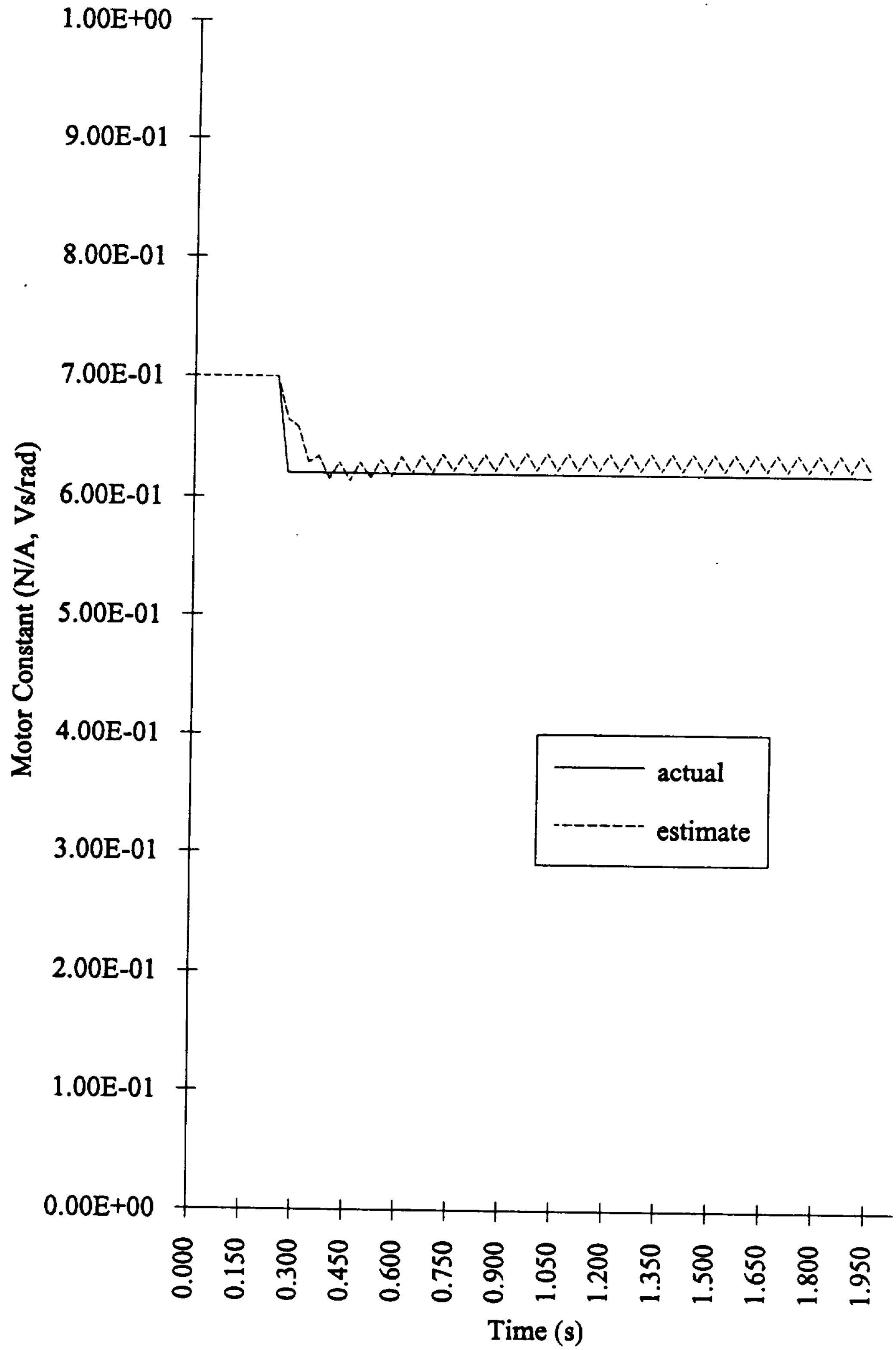

Figure IV.4. Actual and Estimated Motor Constant.

V. EXPERIMENTS

The original plans for mechanically oriented experiments have not changed much since the original planning of the tests except that some additional tests are now being considered because of the availability of the same bearing stack as is used by the NASA actuator. Also, the work being done in fault detection and actuator selection has led to the planning of additional experiments.

V.1. Transient Loading Experiments

Axial loads of various frequencies and magnitudes must be applied to study the effects of startup transient loads on the bearing system, to determine the ability of the actuator to be backdriven, and to study the load accomodating control system. In order for these experiments to be conducted, a system for loading the actuator with a hydraulic cylinder is under development. It is intended to apply a load profile similar to those obtained from the TTB tests as shown in Figure V.1 below. The magnitude of force applied will be small in the first tests but ultimately loads of the kind shown in the figure will be tested. For loads above roughly 25 kips the nut will be prevented from transverse motion to avoid buckling of the screw. This may cause some loss of resolution in the measurement of reaction torques. The conditions of the bearings will be carefully monitored for deterioration due to loading. The heavy loading experiments will be performed as late as is convenient for NASA to prevent damage to the roller screw or main bearings that would jeopardize other experiments.

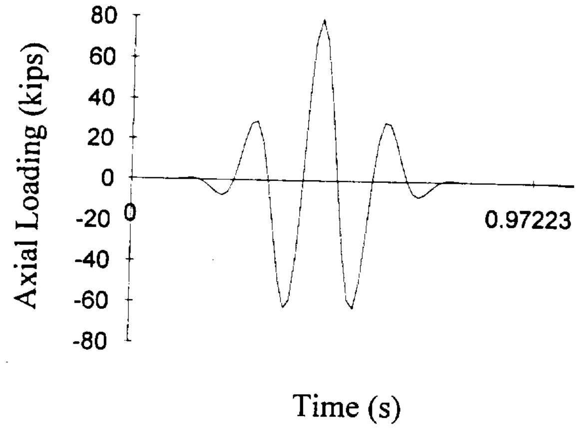

Figure V.1. Experimental Axial Loading Profile.

V.2. Transverse Loading Experiment

This particular experiment requires that side loading be applied to the actuator. The side load will be applied using a spring loaded system that will be carried between the linear bearings. Both cantilever loading and end supported loadings of the screw are possible though cantilevered loading is now intended because of the added similarity to the actuator configuration. Other requirements of this test include measuring the transverse deflections of the screw and the torque seen by the nut. The transverse deflections of the screw will be obtained by mounting a LVDT on the linear bearing perpendicular to the screw. Also, the torque seen by the nut will be measured by using a torque arm and load cell combination. This will be accomplished by placing load cells at the point of contact between the torque arms rigidly attached to the nut and the transverse slide attached to the carrier riding on the linear bearings.

V.3. Friction Experiment

For the friction experiments, the key factors are the measurement of rotary and axial displacements, and torque. Rotary displacement will be measured with a rotary encoder geared or mounted to the main shaft. For the axial displacement, an LVDT will be mounted between the end beam and the nut cage. Greater sensitivity can be obtained using an accelerometer and this may be done. Also, for the applied torque measurements, an in-line torque sensor will be used to measure response to small applied torques.

V.4. Motor Performance Experiment

This experiment will investigate our previous theoretical conclusions concerning efficiency comparisons between brushless dc and induction motors as prime movers in a realistic actuation environment. The keyed screw end provides for easy coupling to a variety of motors. The positioning of the screw end over one of the cement tables offers readily available motor support. Additionally, motor drive efficiencies can be evaluated. The computer data acquisition and control system will be utilized not only for measurement assimilation, but for control output as well (i.e. field-oriented control transformations).

V.5. Health Monitoring and Fault Management Experiment

This experiment will be the first test of prototypical hardware for health monitoring and fault management of brushless dc motors operating under realistic loading. We are currently researching motor vendors and investigating employing a motor drive that will be constructed in-house with IGBTs.

APPENDIX A

Detailed Drawings

TOLERANCES ON: FRACTIONS ±.015 DECIMALS .XXX=±.003
UNLESS OTHERWISE SPECIFIED

DWG. #	REQD.	DESCRIPTION
2	1	TOP SIDE BEAM
3	1	BOTTOM SIDE BEAM
4	1	LEFT END BEAM ASSEMBLY
5	1	RIGHT END BEAM ASSEMBLY

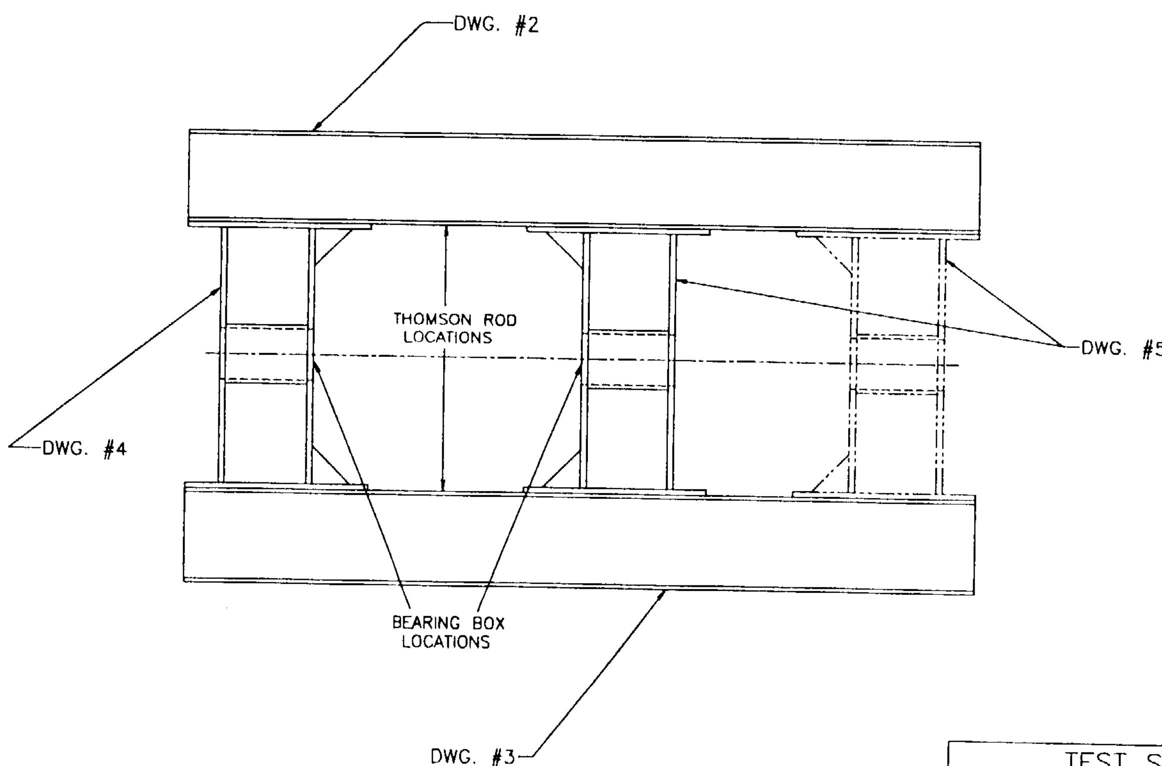

REV.	BY	DESCRIPTION	DATE

REFERENCE

TEST STAND		
DR KSC	PLAN VIEW	
CHD		
DATE	DRAWING NUMBER	REV
SCALE	1	

MATERIAL	DESCRIPTION
STEEL	I-BEAM W12x87 X 108" LG.

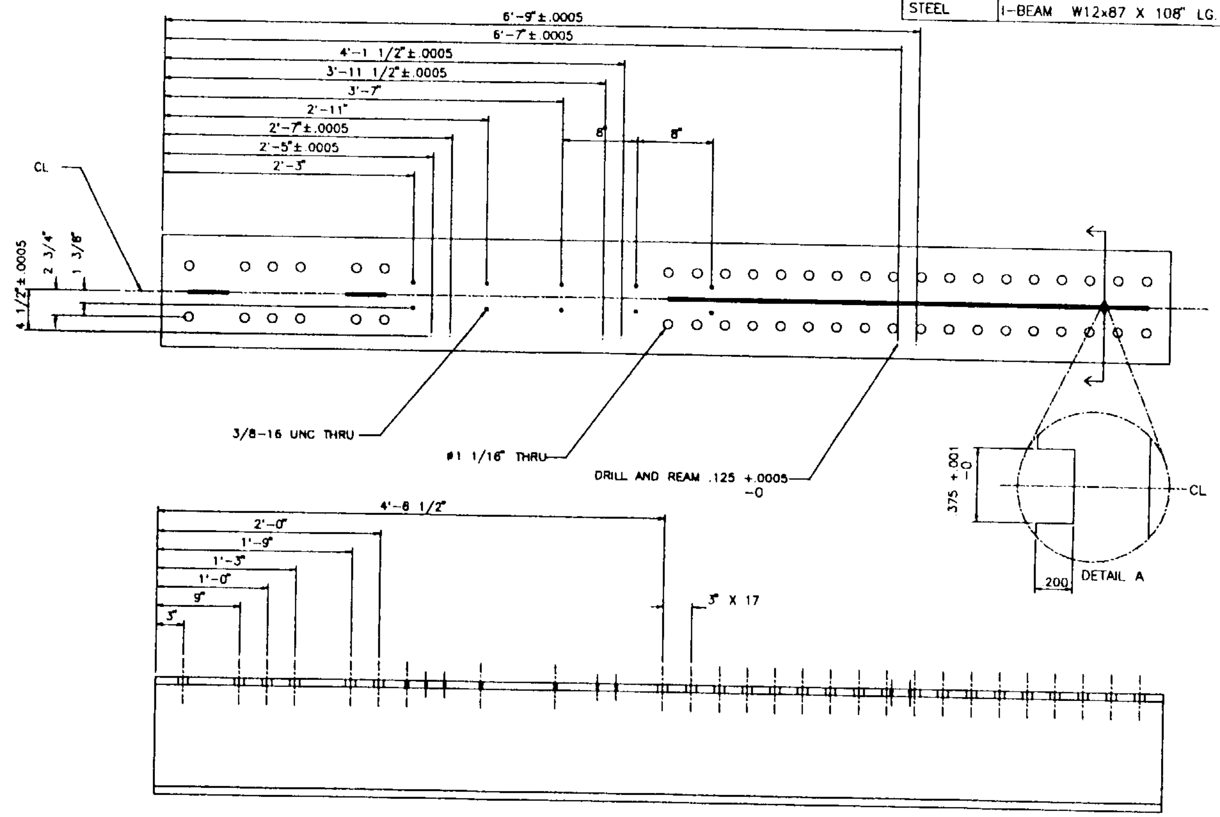

DR. KSC	TEST STAND	
CHD.	TOP SIDE BEAM	
DATE	DRAWING NUMBER	REV
SCALE	2A	

REV	BY	DESCRIPTION	DATE

MATERIAL	DESCRIPTION
STEEL	I-BEAM W12x87 X 108" LG.

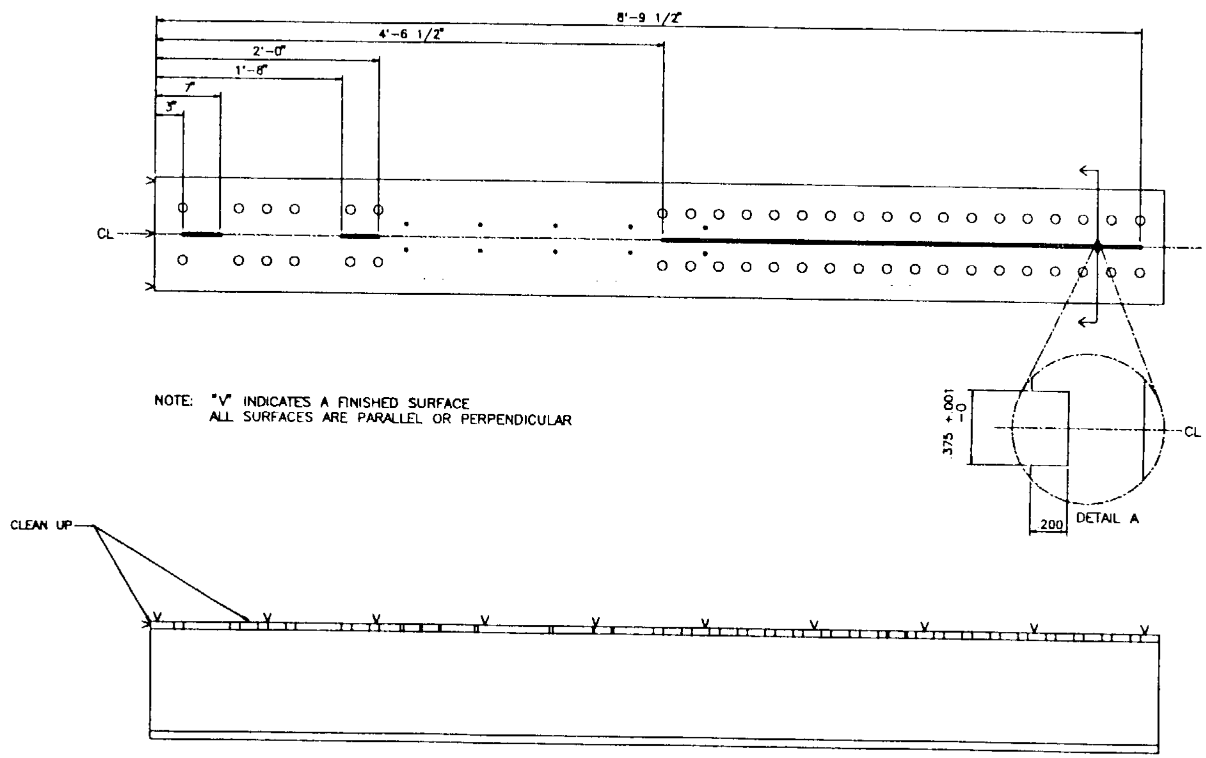

NOTE: "V" INDICATES A FINISHED SURFACE
ALL SURFACES ARE PARALLEL OR PERPENDICULAR

REV.	BY	DESCRIPTION	DATE

TEST STAND	
DR KSC CHD	TOP SIDE BEAM
DATE	DRAWING NUMBER / REV
SCALE	2B

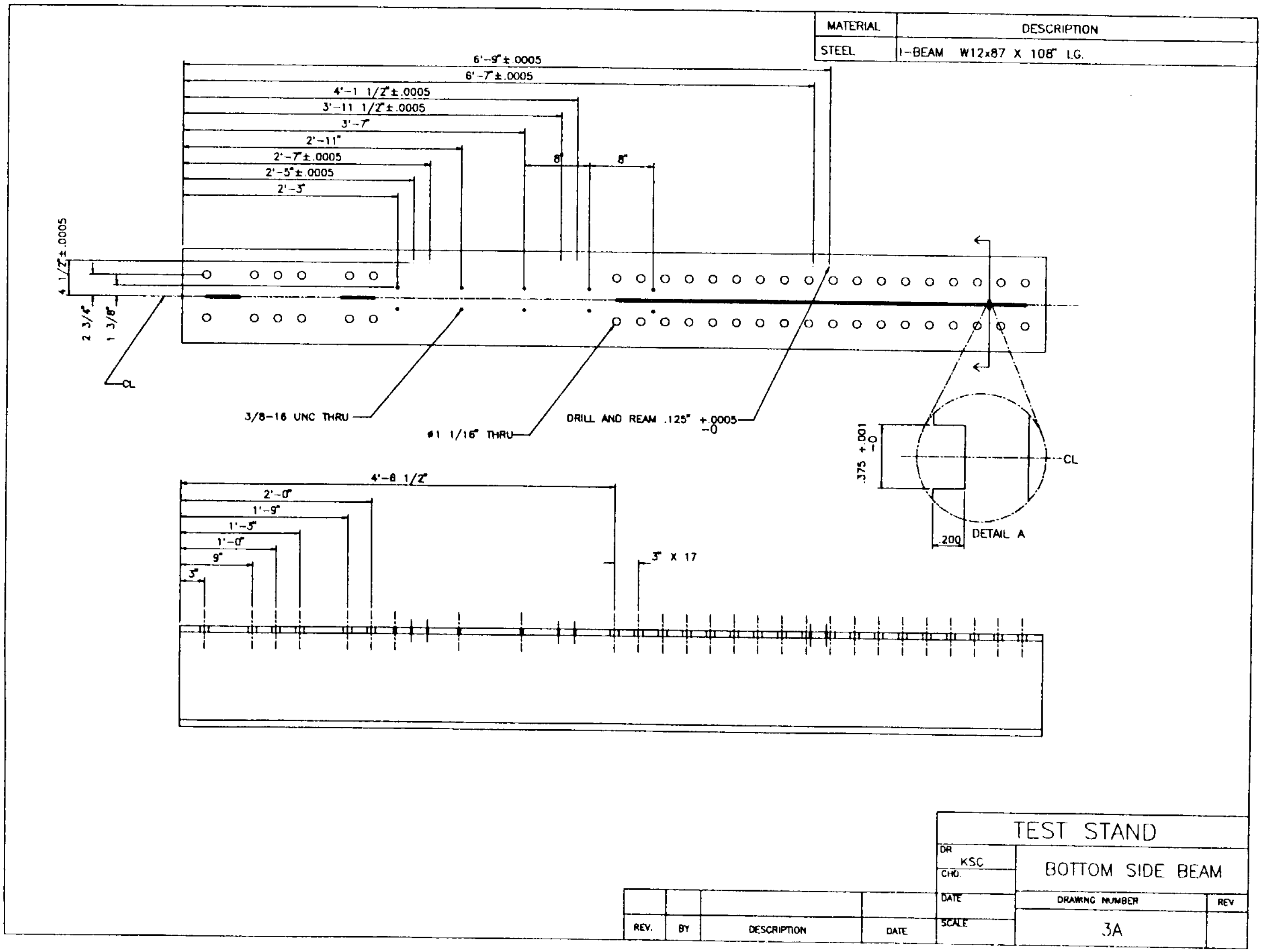

MATERIAL
DESCRIPTION
STEEL
I-BEAM W12x87 X 108" LG.
6'-9" ± .0005
6'-7" ± .0005
4'-1 1/2" ± .0005
3'-11 1/2" ± .0005
3'-7"
2'-11"
2'-7" ± .0005
2'-5" ± .0005
2'-3"
8"
8"
4 1/2" ± .0005
2 3/4"
1 3/8"
CL
3/8-16 UNC THRU
#1 1/16" THRU
DRILL AND REAM .125" +.0005 -0
.375 +.001 -0
CL
.200
DETAIL A
4'-8 1/2"
2'-0"
1'-9"
1'-5"
1'-0"
9"
3"
3" X 17
TEST STAND
DR
KSC
CHD.
BOTTOM SIDE BEAM
DATE
DRAWING NUMBER
REV
SCALE
3A
REV.
BY
DESCRIPTION
DATE

MATERIAL	DESCRIPTION
STEEL	I-BEAM W12x87 X 108" LG.

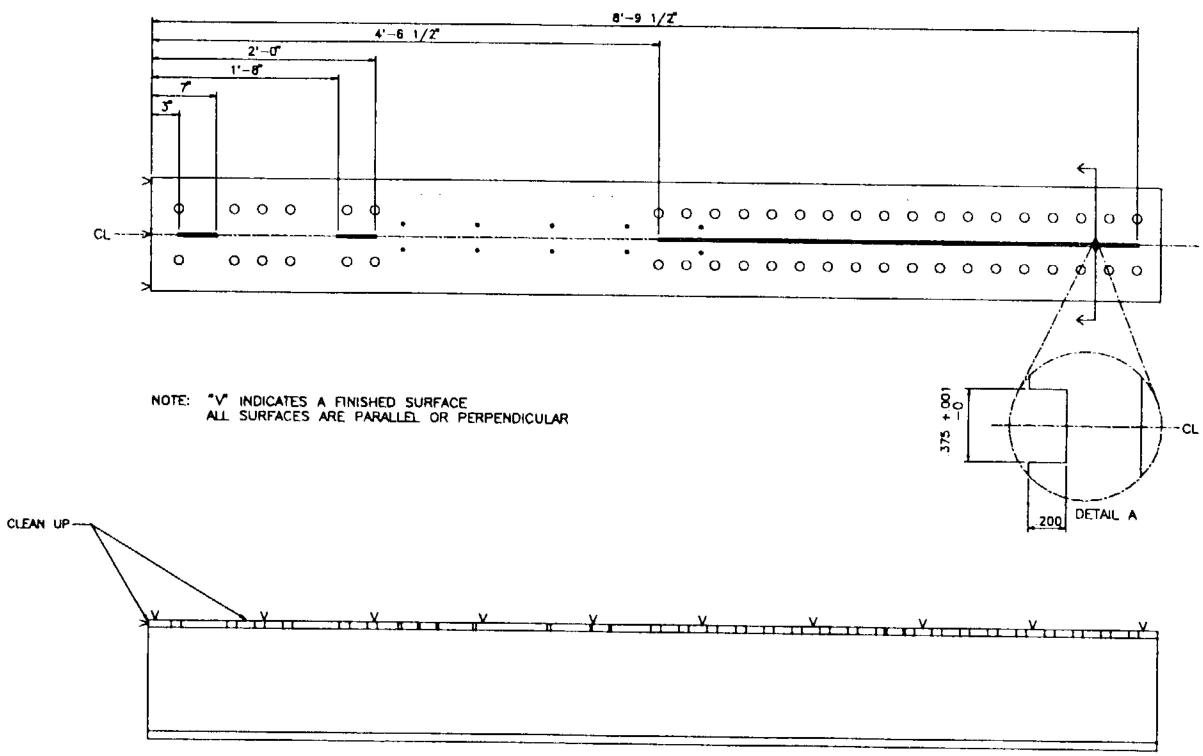

NOTE: "V" INDICATES A FINISHED SURFACE
ALL SURFACES ARE PARALLEL OR PERPENDICULAR

REV.	BY	DESCRIPTION	DATE

TEST STAND

BOTTOM SIDE BEAM

DR KSC

CHD

DATE

SCALE

DRAWING NUMBER: 3B

REV

DWG. #	REQD	DESCRIPTION
6	1	END BEAM
7	2	END PLATES
10	2	GUSSETS

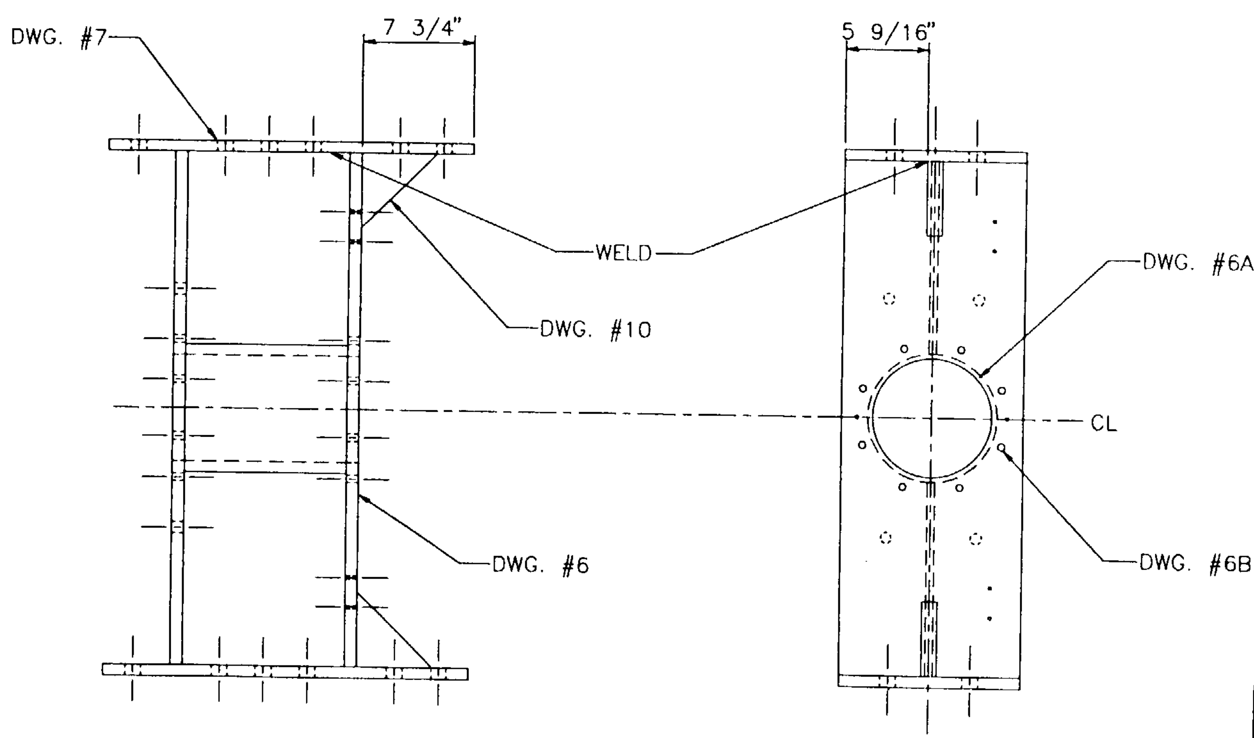

REV	BY	DESCRIPTION	DATE

REFERENCE

TEST STAND

DR KSC

CHD

DATE

SCALE

LEFT END BEAM ASSEMBLY

DRAWING NUMBER 4A

REV

DWG. #	REQD	DESCRIPTION
6	1	END BEAM
7	2	END PLATES
10	2	GUSSETS

NOTE: "V" INDICATES A FINISHED SURFACE.
ALL SURFACES ARE PARALLEL OR PERPENDICULAR

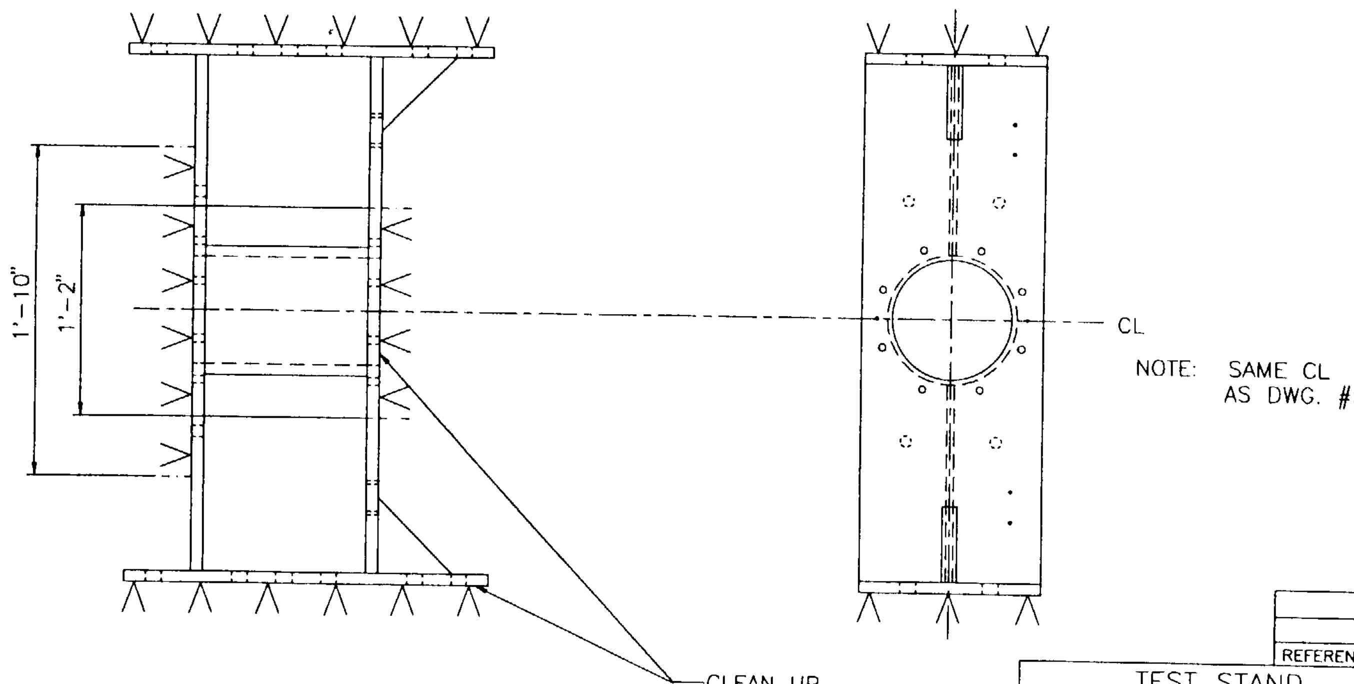

REFERENCE	

				TEST STAND		
				DR KSC	LEFT END BEAM ASSEMBLY	
				CHD		
				DATE	DRAWING NUMBER	REV
REV	BY	DESCRIPTION	DATE	SCALE	4B	

DWG. #	REQD	DESCRIPTION
6	1	END BEAM
7	2	END PLATES
10	2	GUSSETS

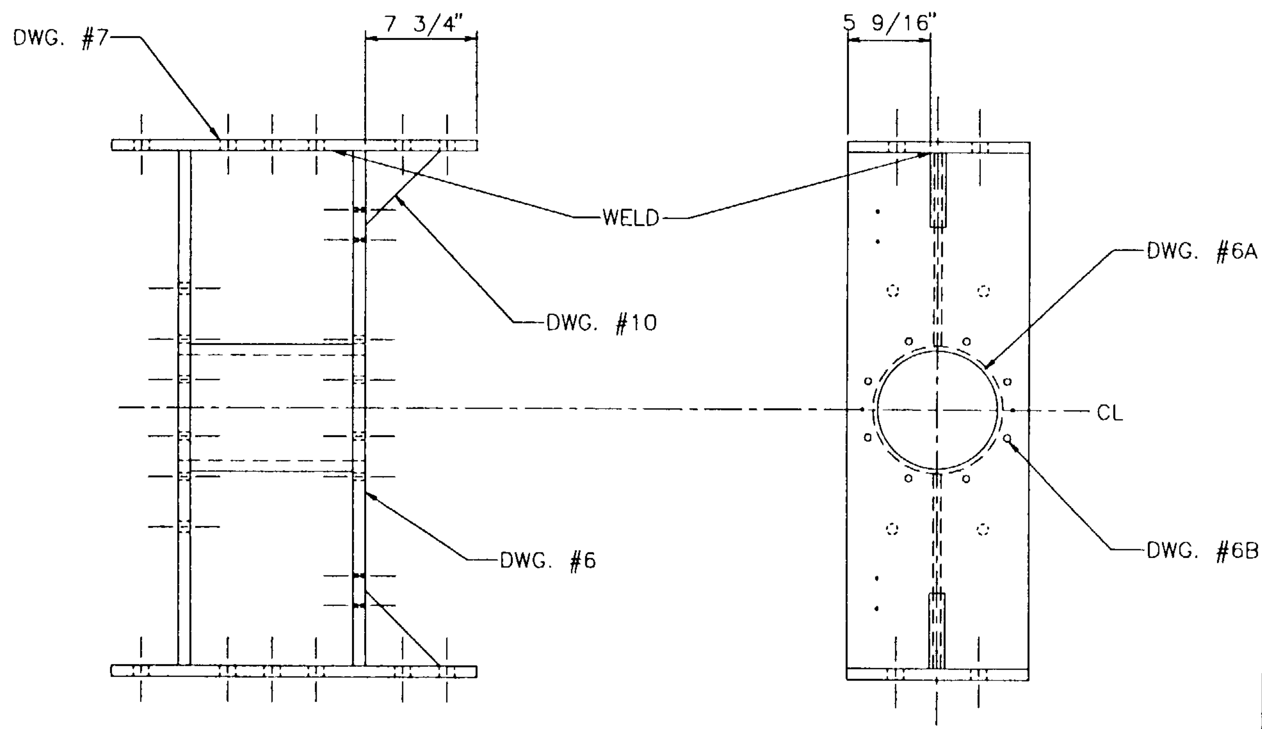

REV.	BY	DESCRIPTION	DATE

REFERENCE

TEST STAND

DR KSC
CHD
DATE
SCALE

RIGHT END BEAM ASSEMBLY

DRAWING NUMBER: 5A

REV

DWG. #	REQD	DESCRIPTION
6	1	END BEAM
7	2	END PLATES
10	2	GUSSETS

NOTE: "V" INDICATES A FINISHED SURFACE.
ALL SURFACES ARE PARALLEL OR PERPENDICULAR

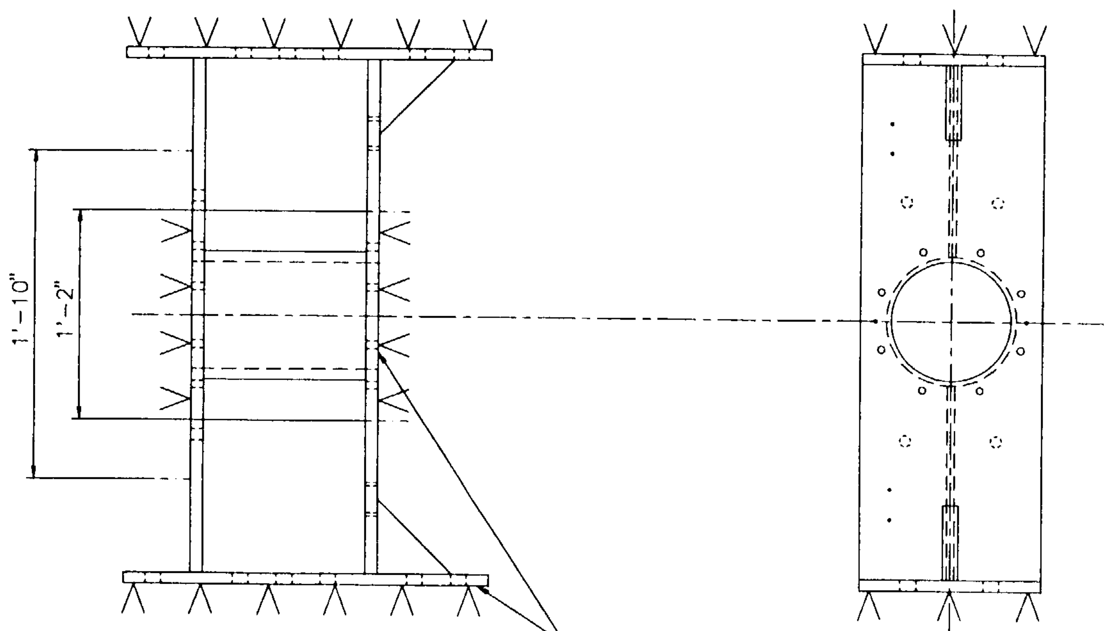

NOTE: SAME CL AS DWG. #4

REV.	BY	DESCRIPTION	DATE

REFERENCE

TEST STAND

RIGHT END BEAM ASSEMBLY

DR KSC

CHD

DATE

SCALE

DRAWING NUMBER 5B

REV

DWG. #	REQD.	DESCRIPTION
8	1	STEEL I-BEAM W12x87 X 36" LG
9	1	8" STEEL PIPE, 1' 1/2" LG

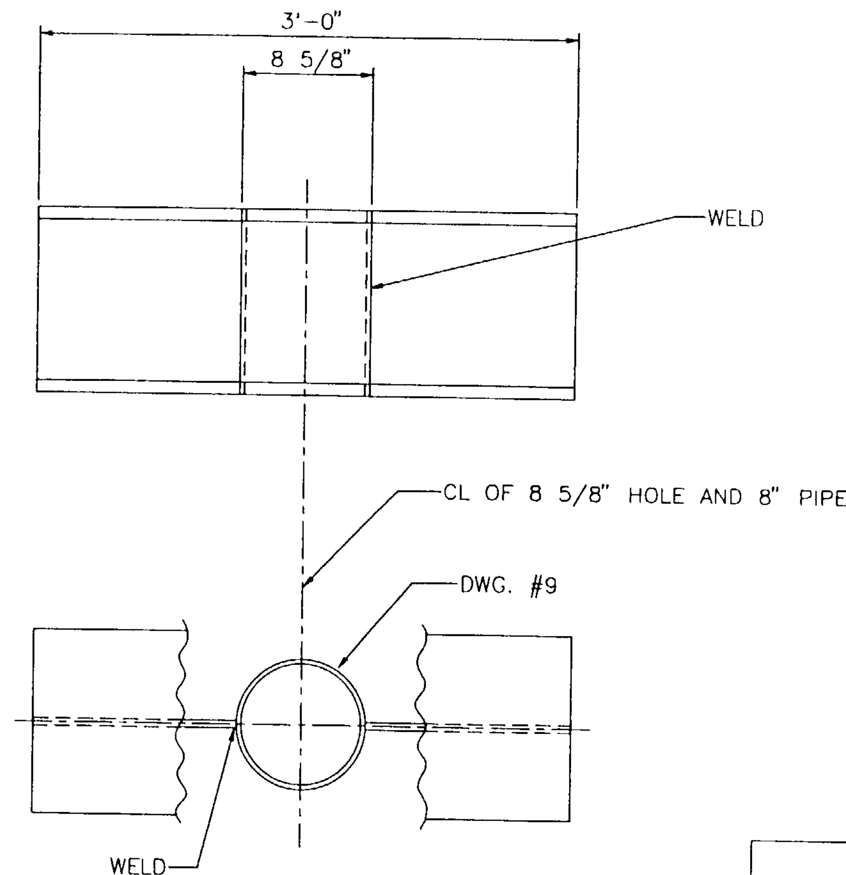

REFERENCE			
TEST STAND			
DR KSC	CHD	END BEAM	
DATE		DRAWING NUMBER	REV
SCALE		6A	

REV.	BY	DESCRIPTION	DATE

DWG. #	REQD.	DESCRIPTION
8	1	STEEL I-BEAM W12x87 X 36" LG
9	1	8" STEEL PIPE, 1' 1/2" LG

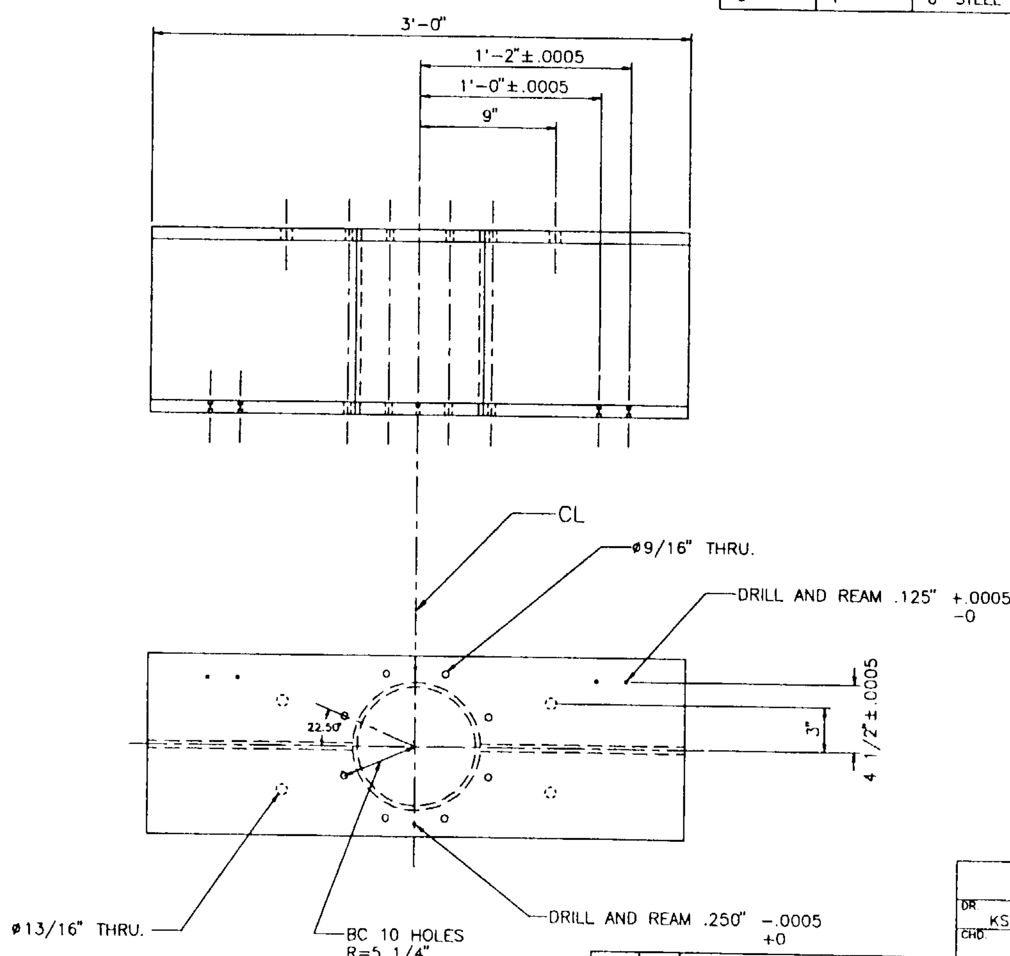

REV.	BY	DESCRIPTION	DATE

REFERENCE

TEST STAND

DR KSC
CHD
DATE
SCALE

END BEAM

DRAWING NUMBER	REV
6B	

MATERIAL	DESCRIPTION
STEEL	PL. 1" X 11-15/16"

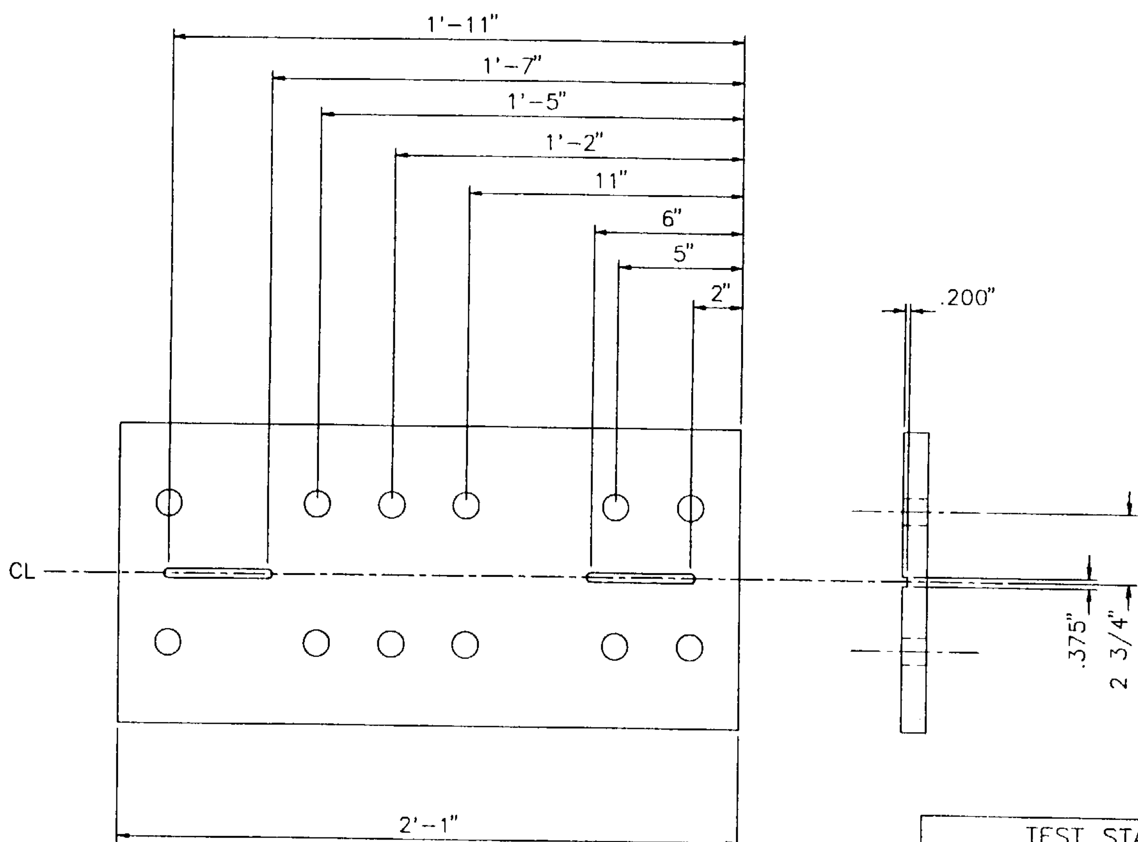

REV.	BY	DESCRIPTION	DATE

	REFERENCE
TEST STAND	
DR KSC / CHD	END PLATE
DATE	DRAWING NUMBER: 7
SCALE	REV

MATERIAL	DESCRIPTION
STEEL	I-BEAM W12x87 X 36" LG.

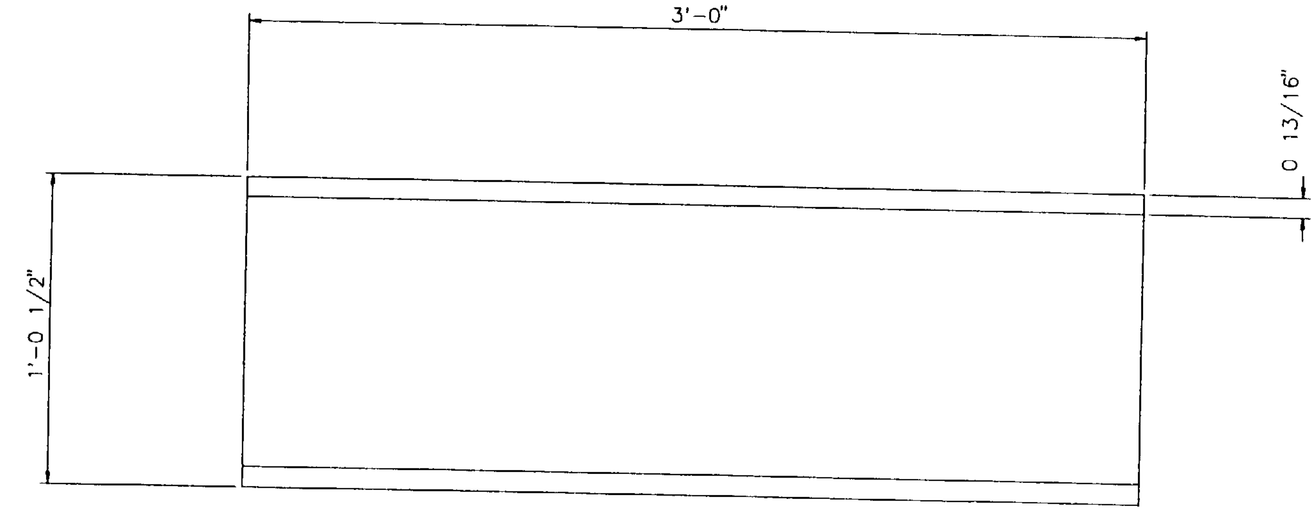

NOTE: 1/2" WEB THICKNESS

REV	BY	DESCRIPTION	DATE

REFERENCE

TEST STAND		
DR KSC	I BEAM	
CHD		
DATE	DRAWING NUMBER	REV
SCALE	8	

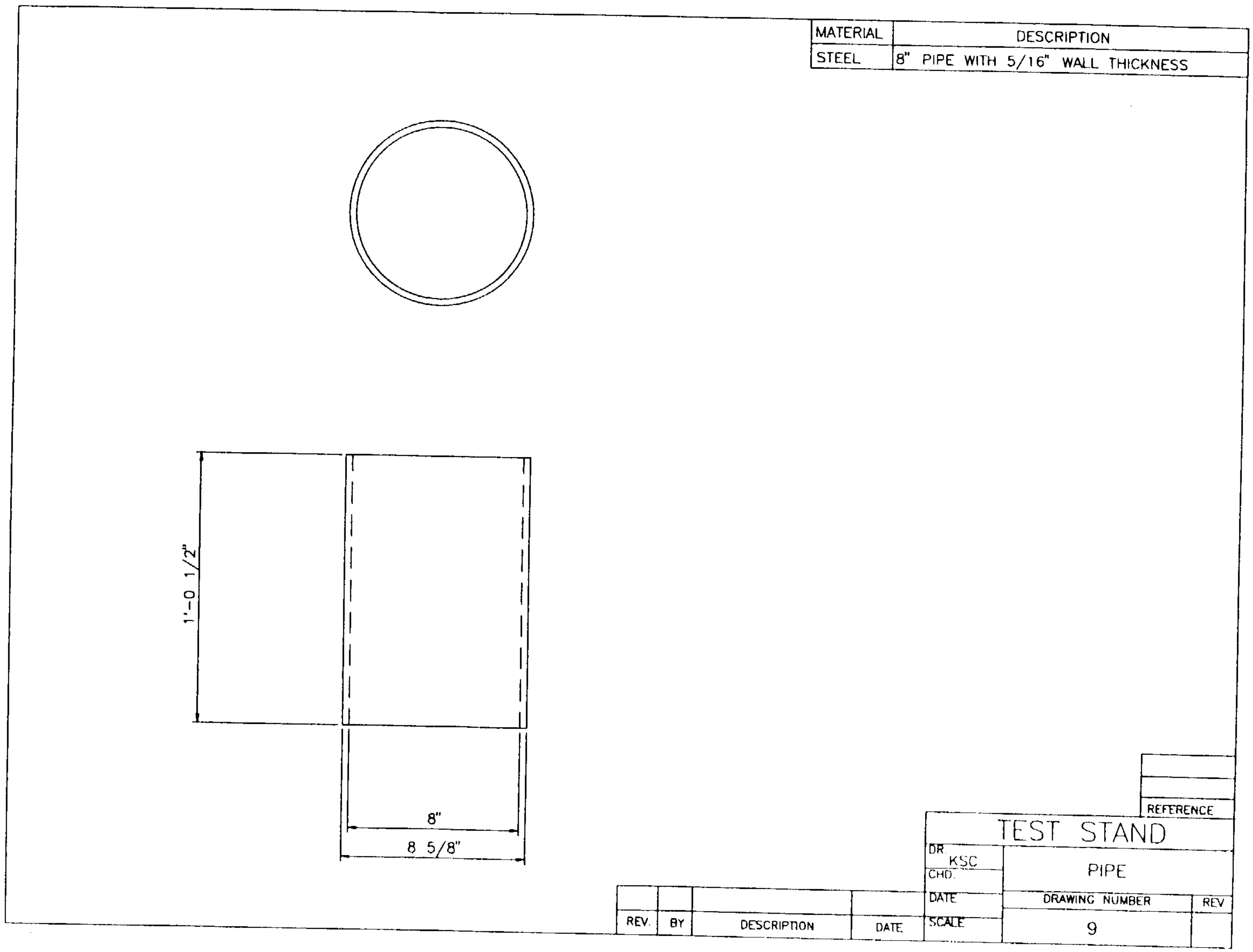
MATERIAL
DESCRIPTION
STEEL
8" PIPE WITH 5/16" WALL THICKNESS
1'-0 1/2"
8"
8 5/8"
REFERENCE
TEST STAND
DR KSC
CHD.
DATE
SCALE
PIPE
DRAWING NUMBER
REV
9
REV.
BY
DESCRIPTION
DATE

MATERIAL	DESCRIPTION
STEEL	PL. 1" X 11-15/16"

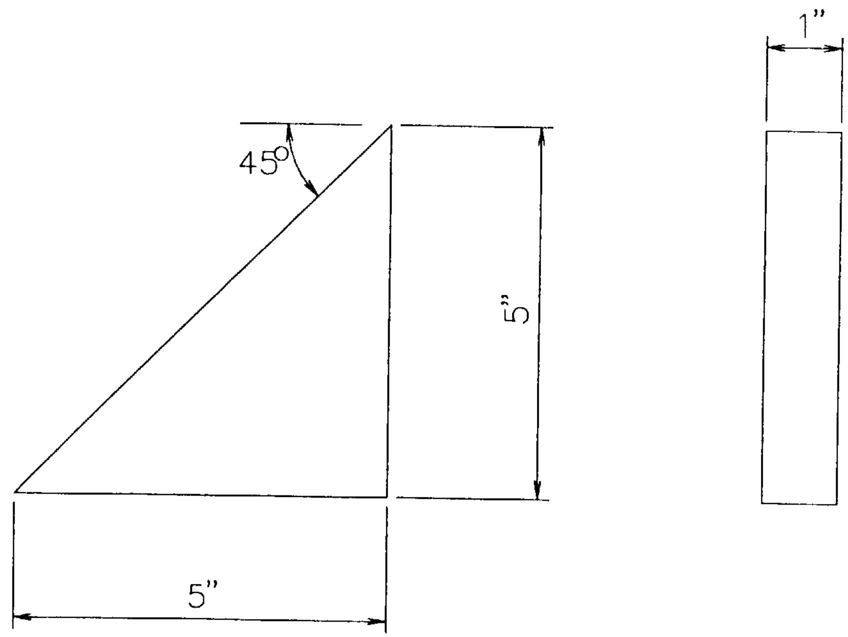

REV.	BY	DESCRIPTION	DATE

REFERENCE

TEST STAND

DR. KSC

CHD.

DATE

SCALE

GUSSET

DRAWING NUMBER	REV
10	

APPENDIX B

Initial Student Drawings

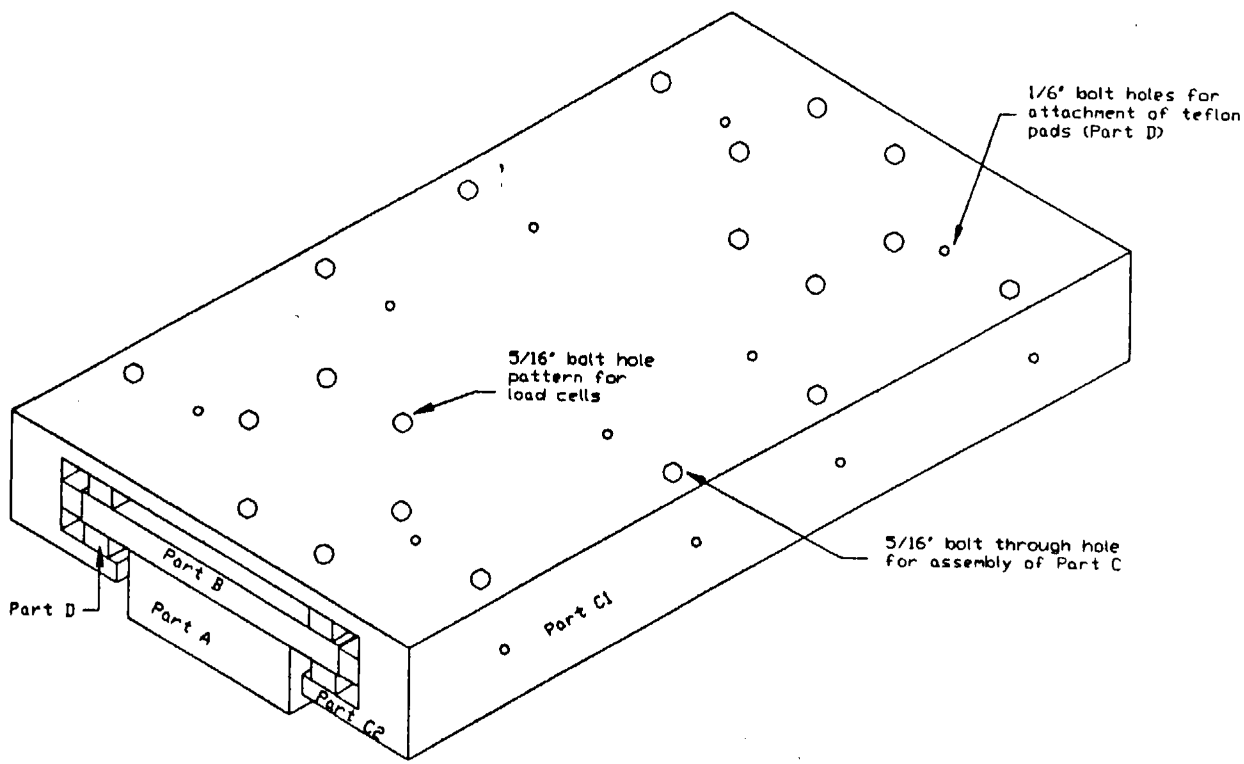

Note: Overall view of slide in completed form. The dimensioned views are provided.

DRAWING:	3-D drawing of entire slide
NAME:	Terry Thorn & Renee' Luttrell
CLASS:	ME 383 Project Design
DATE:	February 18, 1994

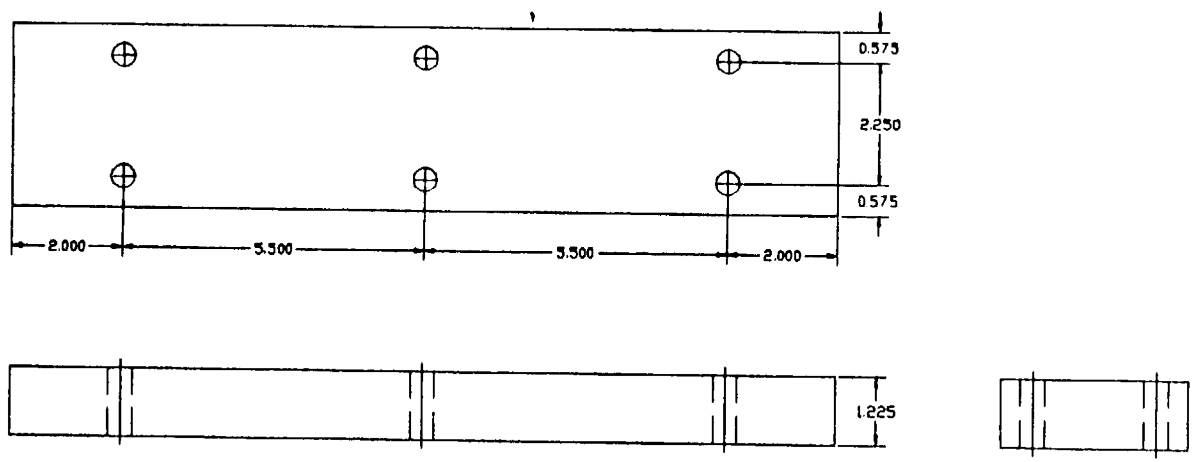

Notes: 6 7/16" through bolt holes
for attaching Part B.

All dimensions in inches.
Tolerances x.xxx ± 0.005

DRAWING:	Part A
NAME:	Terry Thorn & Renee' Luttrell
CLASS:	ME 383 Project Design
DATE:	February 18, 1994

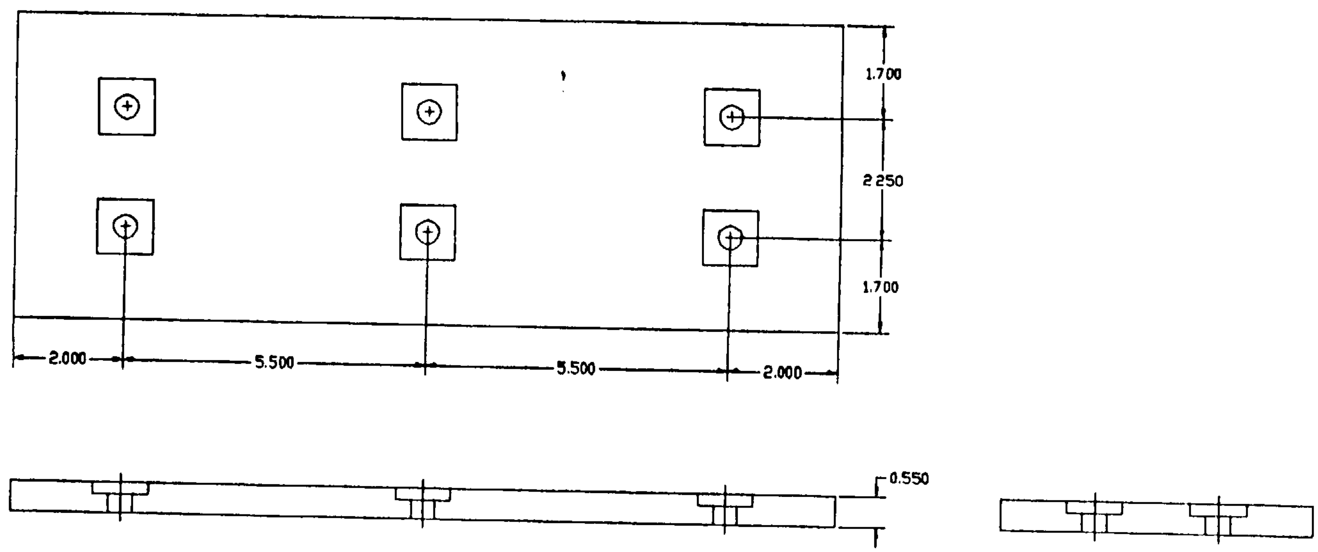

Notes: 6 7/16' countersunk through bolt holes for attaching Part A.

All dimensions in inches.
Tolerances x.xxx ± 0.005

Smooth finish required in order to slide against teflon pads.

DRAWING:	Part B
NAME:	Terry Thorn & Renee' Luttrell
CLASS:	ME 383 Project Design
DATE:	February 18, 1994

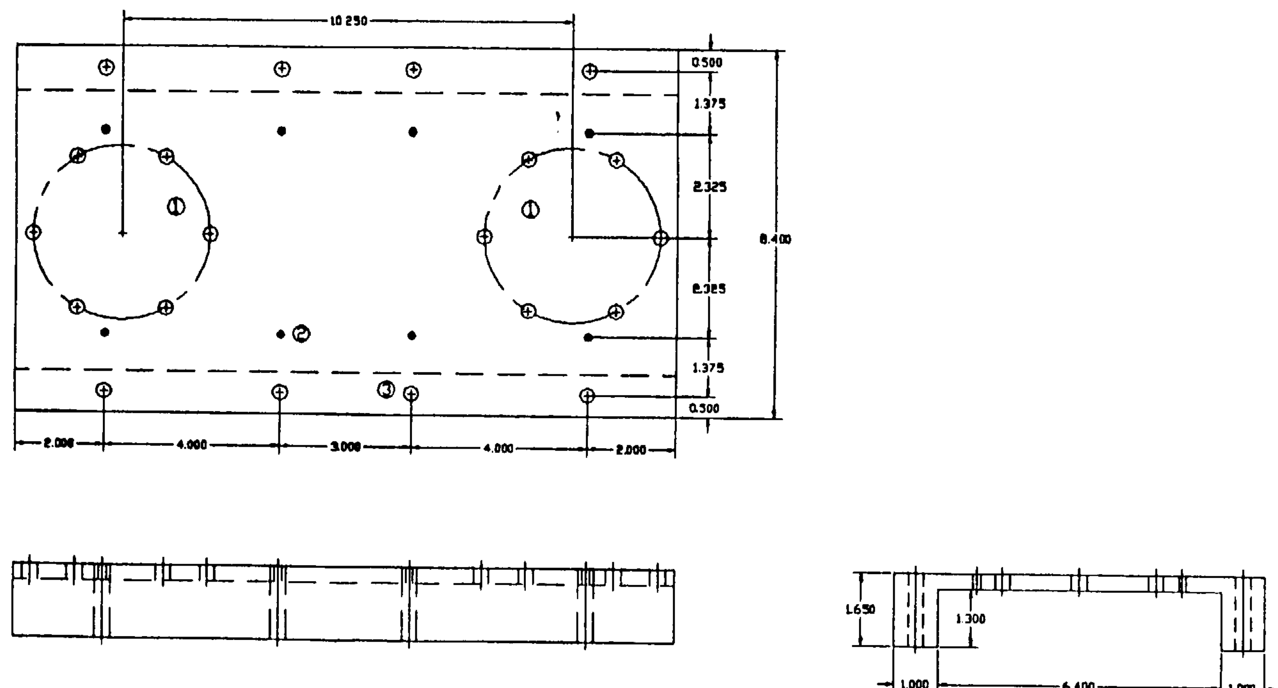

Notes: ① 6 5/16" through bolt holes evenly spaced.
② 8 1/6" through bolt holes to attach teflon pads.
③ 8 5/16" through bolt holes to assemble slide.

All dimensions in inches.
Tolerances x.xxx ± 0.005

DRAWING: Part C1

NAME: Terry Thorn & Renee' Luttrell
CLASS: ME 383 Project Design
DATE: February 18, 1994

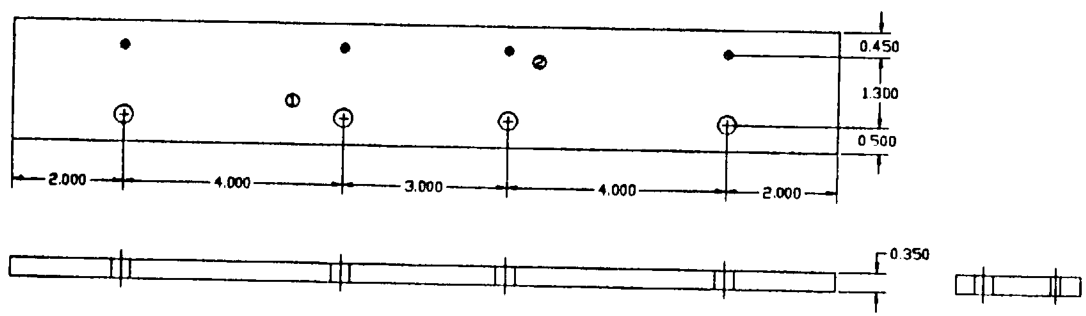

Notes: ① 4 5/16' through bolt holes for assembly with Part C1.
② 4 1/6' through bolt holes for attaching the teflon pads.

All dimensions in inches.
Tolerances x.xxx ± 0.005
Produce 2 pieces

DRAWING:	Part C2
NAME:	Terry Thorn & Renee' Luttrell
CLASS:	ME 383 Project Design
DATE:	February 18, 1994

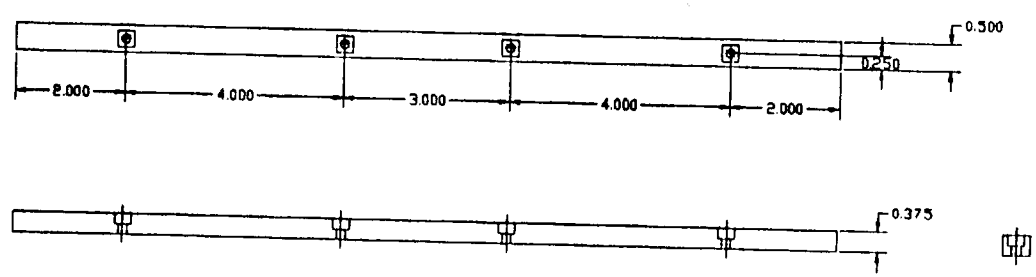

Notes: 4 1/6' through bolt holes
for attaching teflon to Part C.

All dimensions in inches.
All tolerances x.xxx ± 0.005

Produce 6 pieces

DRAWING:	Part D (teflon pads)
NAME:	Terry Thorn & Renee' Luttrell
CLASS:	ME 383 Project Design
DATE:	February 18, 1994

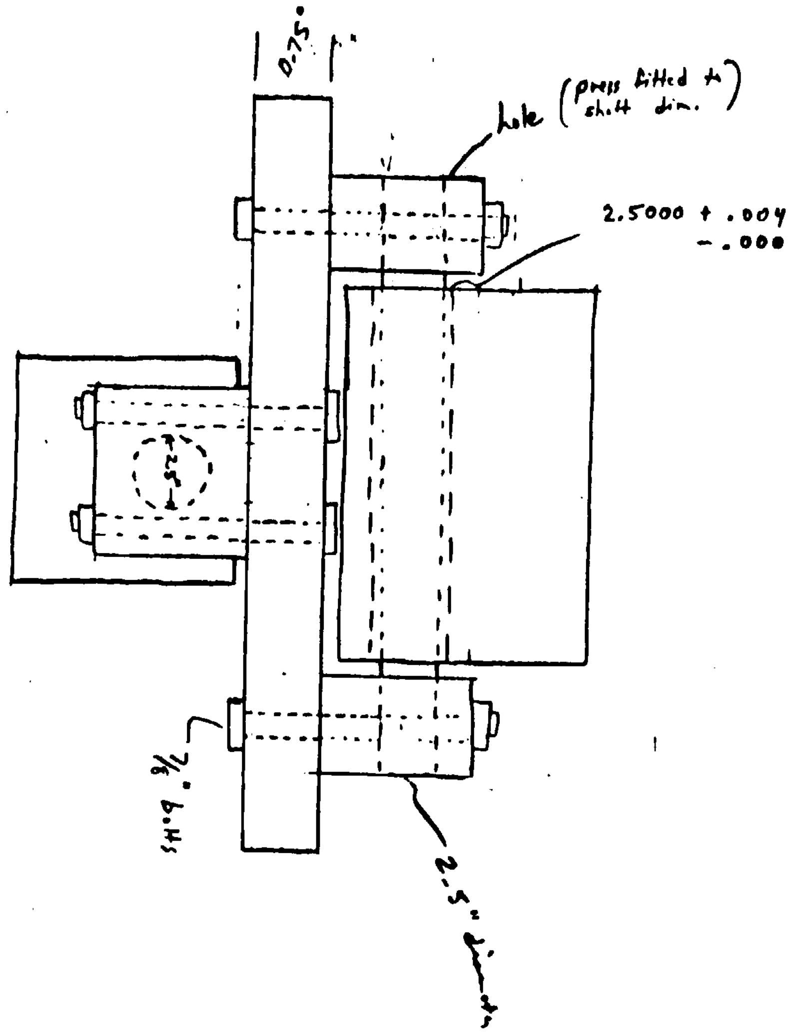

NOTE.
Shaft tolerance (Class L)
2.4993/2.4985

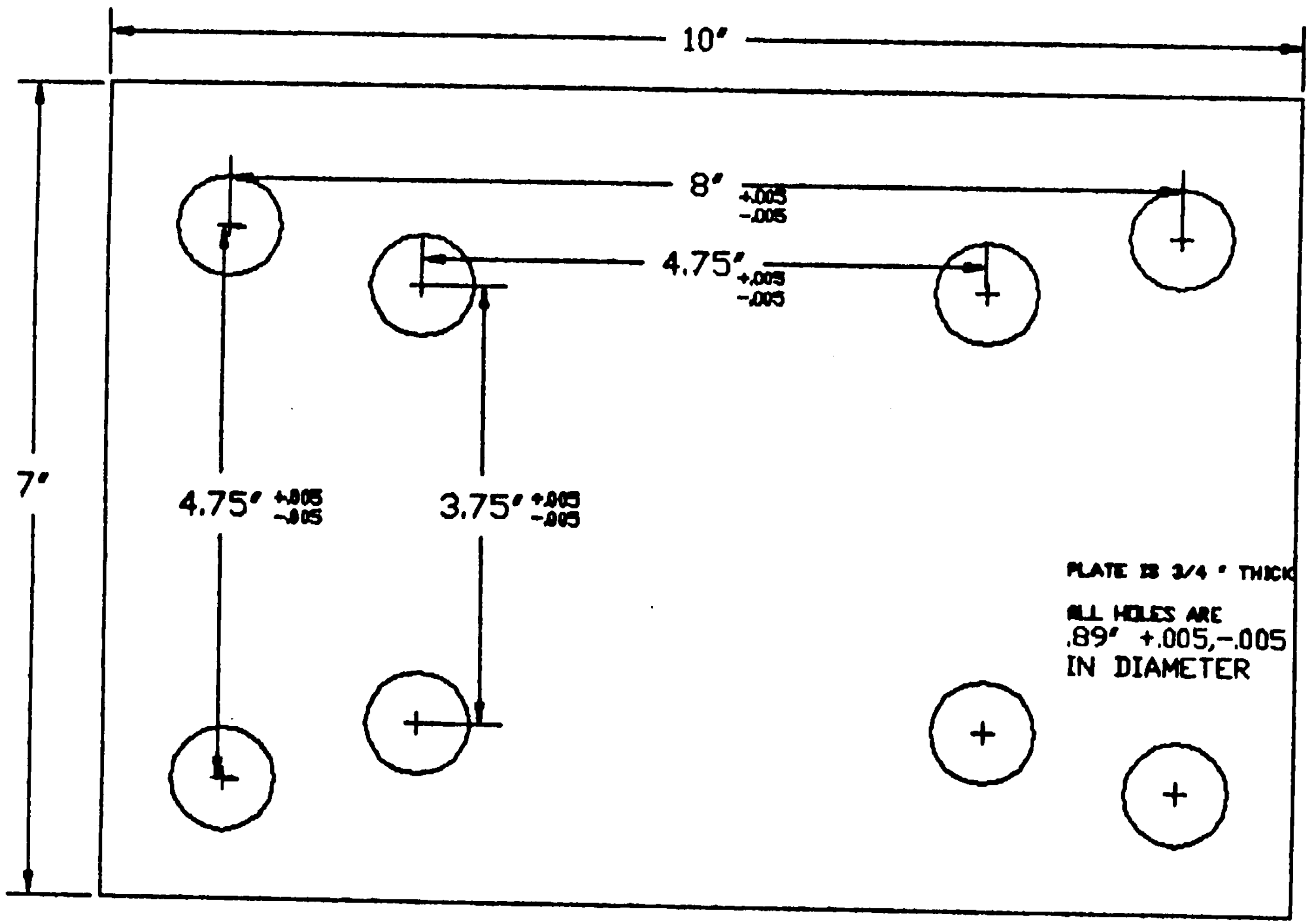
10″
7″
8″ +.005 -.005
4.75″ +.005 -.005
4.75″ +.005 -.005
3.75″ +.005 -.005
PLATE IS 3/4 ″ THICK
ALL HOLES ARE
.89″ +.005,-.005
IN DIAMETER

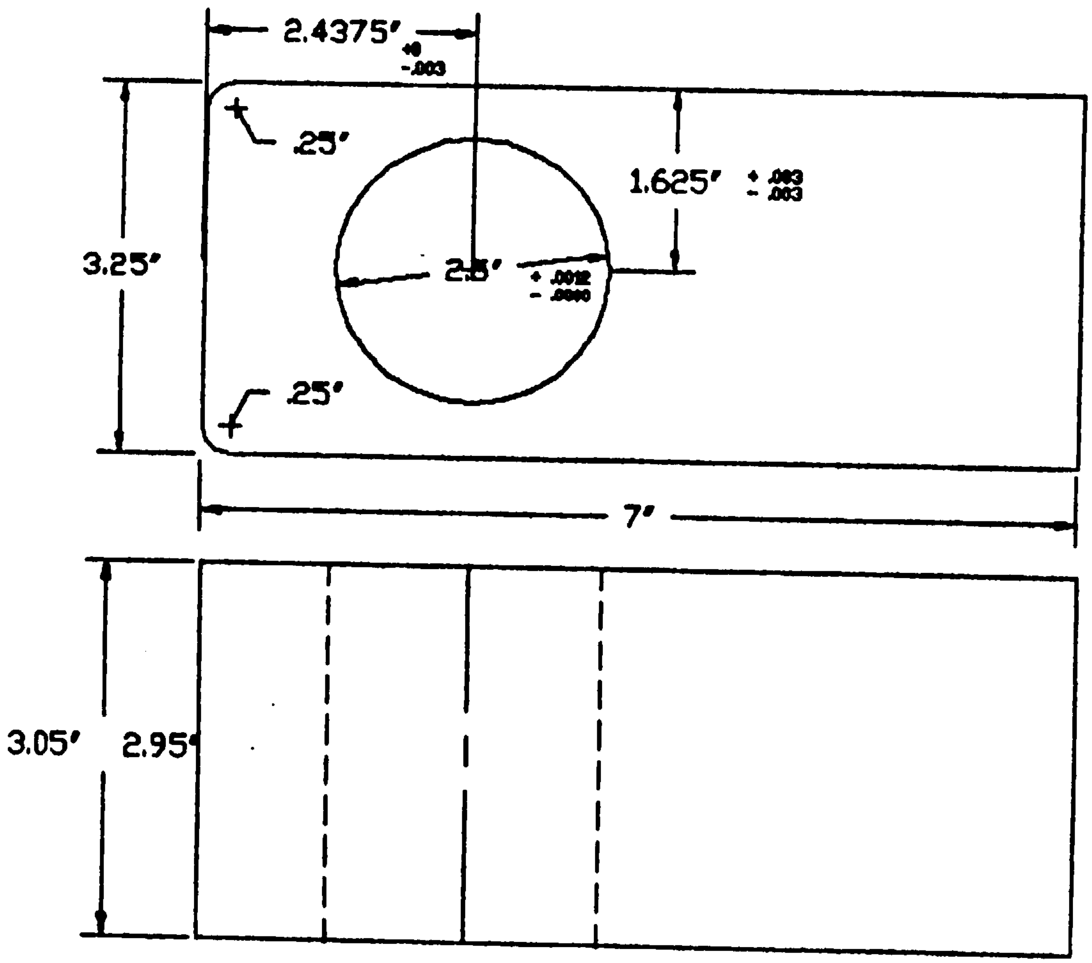

COUPLING ARM
QUANTITY = 2

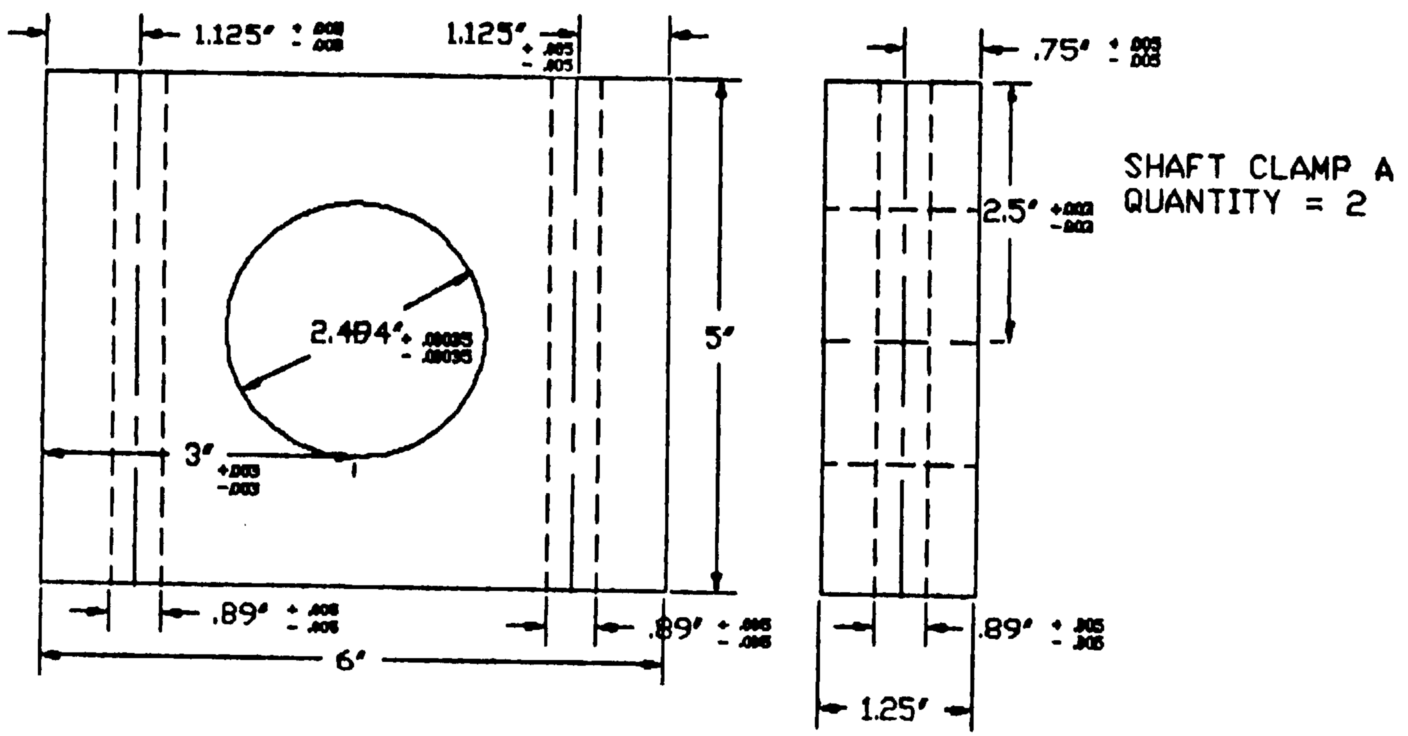
1.125″ ± .008
1.125″ ± .005
.75″ ± .005
SHAFT CLAMP A
QUANTITY = 2
2.5″ ± .002
2.494″ ± .00035
5″
3″ ± .003
.89″ ± .005
.89″ ± .005
.89″ ± .005
6″
1.25″

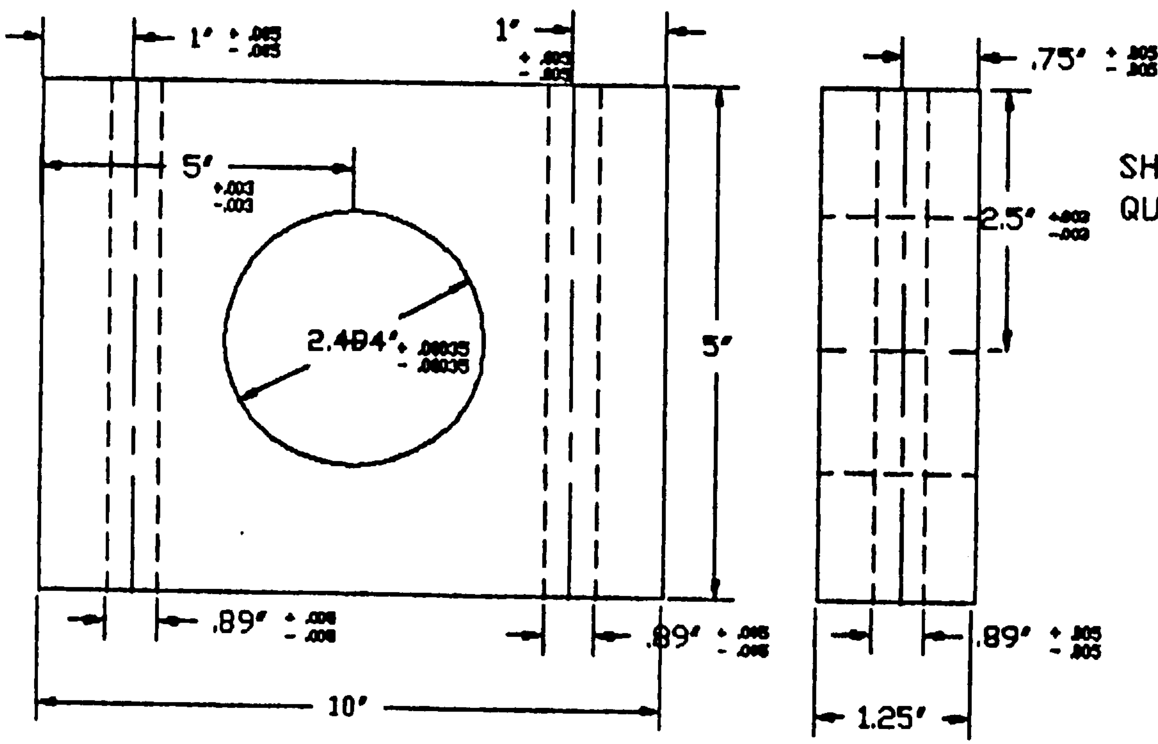

SHAFT CLAMP B
QUANTITY = 2

SPRING MECHANISM

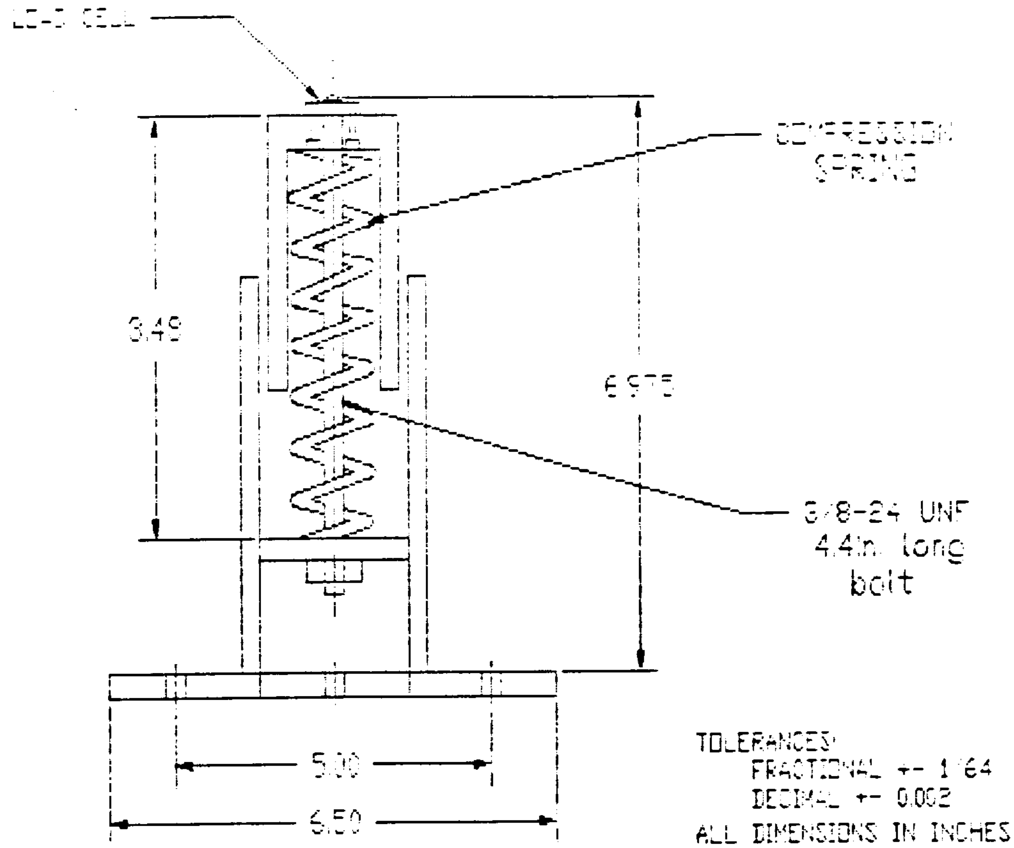

ORIGINAL PAGE IS
OF POOR QUALITY

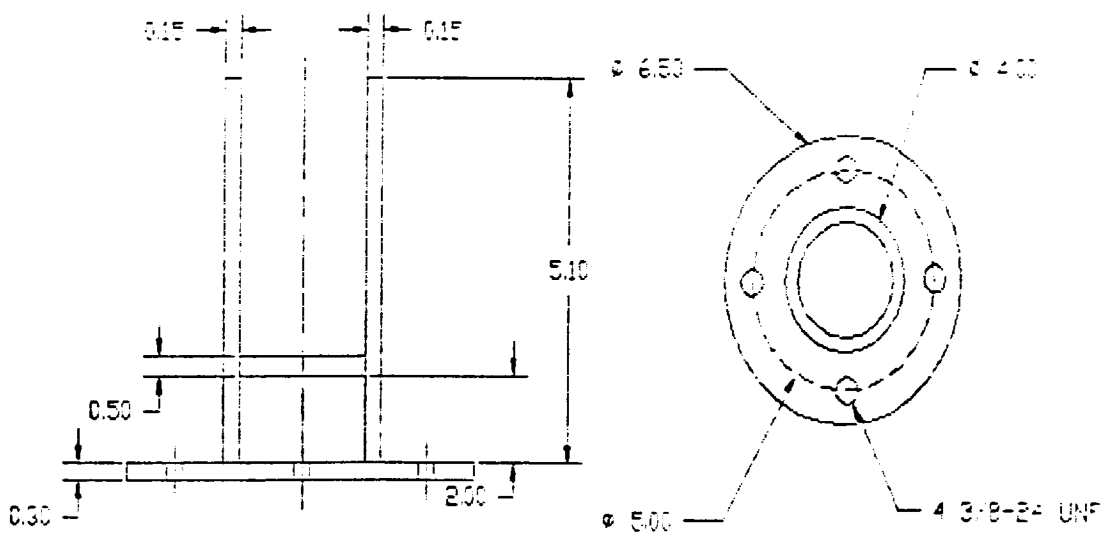
0.15
0.15
5.10
0.50
0.30
2.00
φ 6.50
φ 4.00
φ 5.00
4 3/8-24 UNF

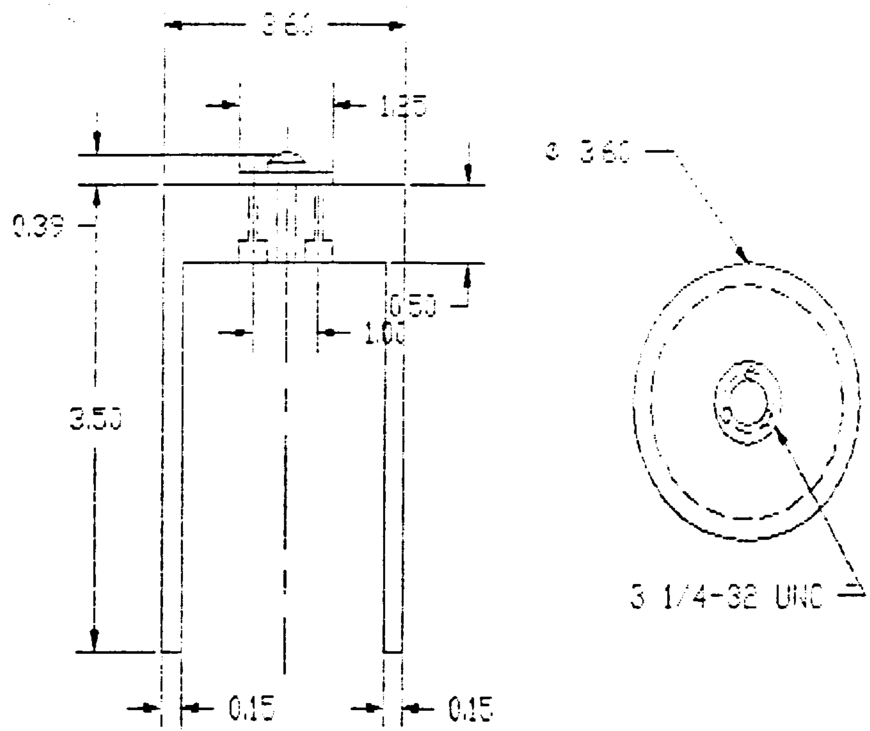
3.60
1.25
0.39
0.50
1.00
3.50
0.15
0.15
Ø 3.60
3 1/4-32 UNC

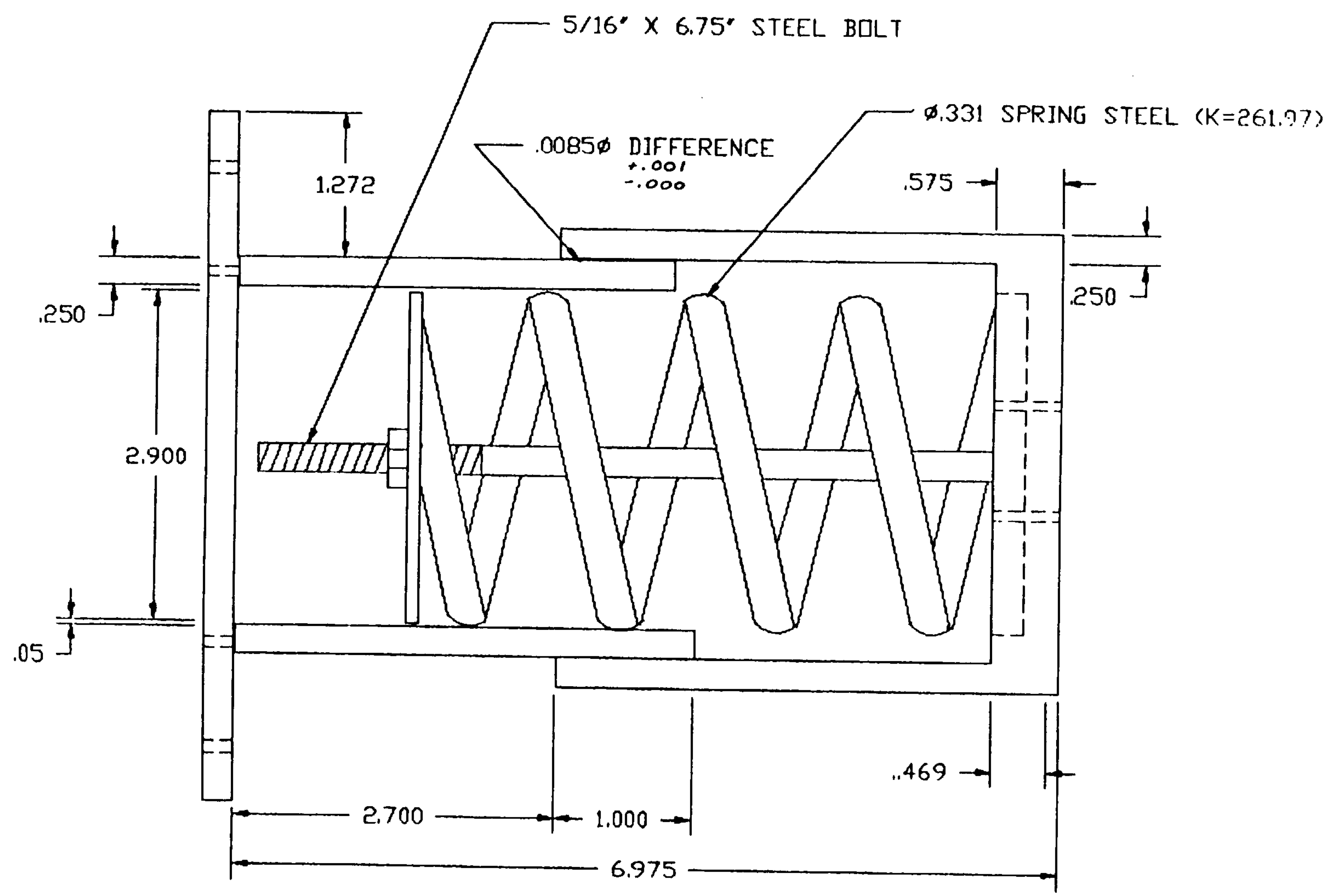

FRONT VIEW

★ All dimensions given ± 1/64 unless otherwise stated.

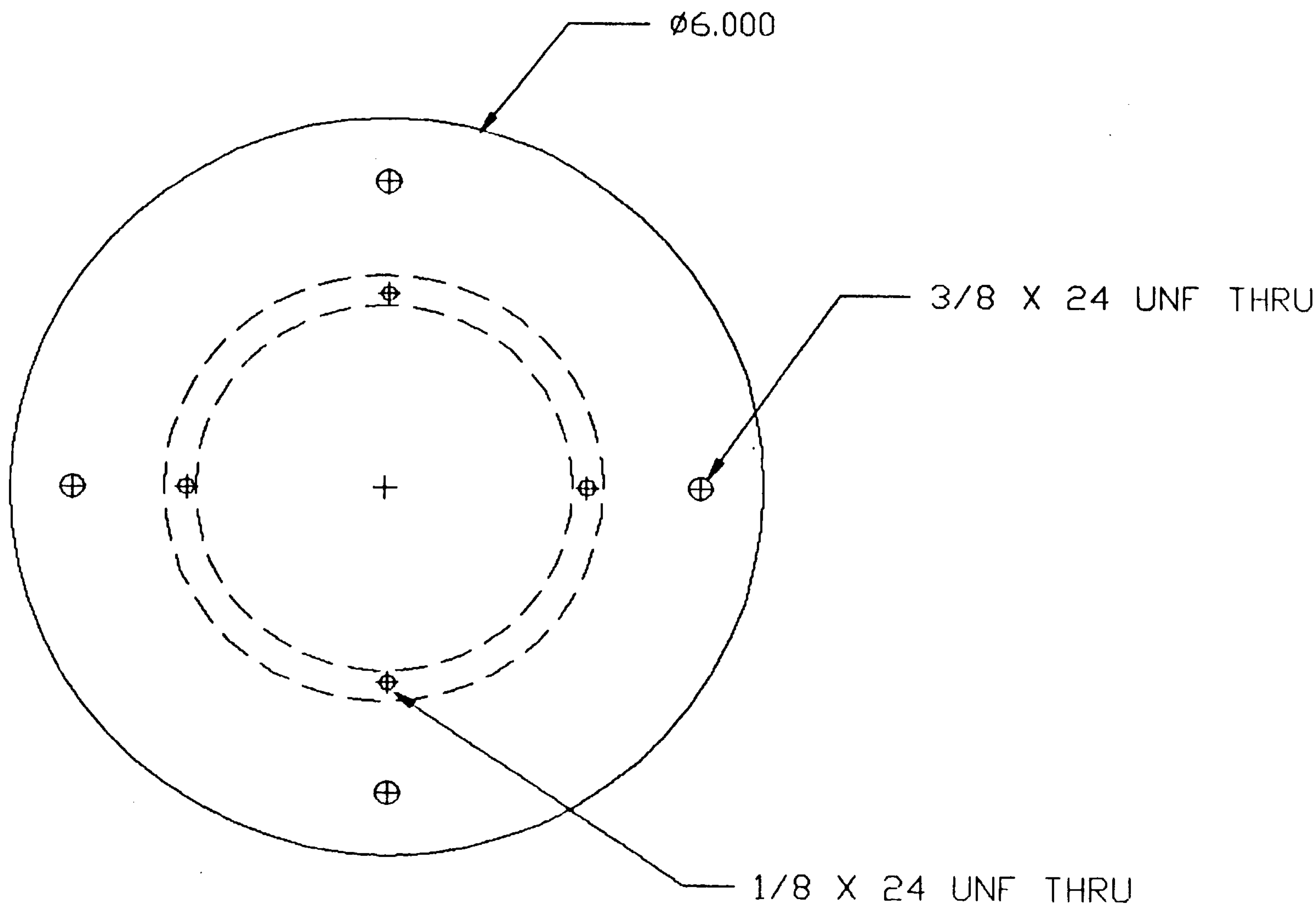

★ All dimensions ± 1/64" unless otherwise stated

LEFT END VIEW

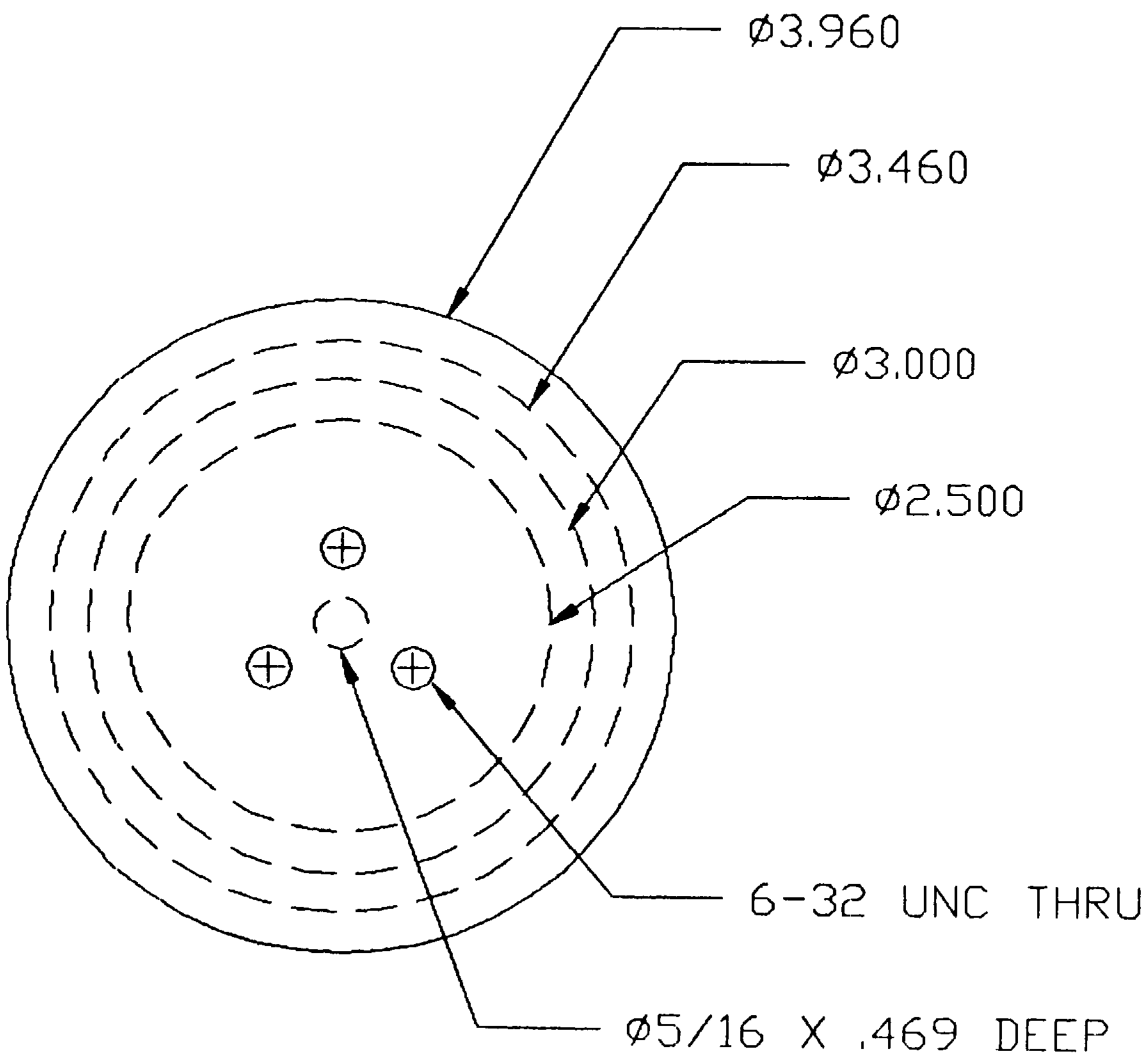

RIGHT END VIEW

* All dimensions ± 1/64" unless otherwise stated